

## Combined CDF and D0 Upper Limits on Standard Model Higgs-Boson Production with up to $6.7 \text{ fb}^{-1}$ of Data

The TEVNPH Working Group\*  
*for the CDF and D0 Collaborations*

*November 18, 2018*

We combine results from CDF and D0 on direct searches for the standard model (SM) Higgs boson ( $H$ ) in  $p\bar{p}$  collisions at the Fermilab Tevatron at  $\sqrt{s} = 1.96 \text{ TeV}$ . Compared to the previous Tevatron Higgs search combination more data have been added, additional new channels have been incorporated, and some previously used channels have been reanalyzed to gain sensitivity. We use the latest parton distribution functions and  $gg \rightarrow H$  theoretical cross sections when comparing our limits to the SM predictions. With up to  $5.9 \text{ fb}^{-1}$  of data analyzed at CDF, and up to  $6.7 \text{ fb}^{-1}$  at D0, the 95% C.L. upper limits on Higgs boson production are factors of 1.56 and 0.68 the values of the SM cross section for a Higgs boson mass of  $m_H = 115 \text{ GeV}/c^2$  and  $165 \text{ GeV}/c^2$ . We exclude, at the 95% C.L., a new and larger region at high mass between  $158 < m_H < 175 \text{ GeV}/c^2$ .

*Preliminary Results*

---

\* The Tevatron New-Phenomena and Higgs Working Group can be contacted at [TEVNPHWG@fnal.gov](mailto:TEVNPHWG@fnal.gov). More information can be found at <http://tevnphwg.fnal.gov/>.

## I. INTRODUCTION

The search for a mechanism for electroweak symmetry breaking, and in particular for a standard model (SM) Higgs boson has been a major goal of particle physics for many years, and is a central part of the Fermilab Tevatron physics program. Both the CDF and D0 collaborations have performed new combinations [1, 2] of multiple direct searches for the SM Higgs boson. The new searches include more data, the inclusion of additional channels, and improved analysis techniques compared to previous analyses. The sensitivities of these new combinations significantly exceed those of previous combinations [3, 4].

In this note, we combine the most recent results of all such searches in  $p\bar{p}$  collisions at  $\sqrt{s} = 1.96$  TeV. The analyses combined here seek signals of Higgs bosons produced in association with vector bosons ( $q\bar{q} \rightarrow W/ZH$ ), through gluon-gluon fusion ( $gg \rightarrow H$ ), and through vector boson fusion (VBF) ( $q\bar{q} \rightarrow q'\bar{q}'H$ ) corresponding to integrated luminosities up to  $5.9 \text{ fb}^{-1}$  at CDF and up to  $6.7 \text{ fb}^{-1}$  at D0. In order to report an integrated luminosity corresponding to the data sample used to make our results, we must average together the contributing searches' luminosities in a way that represents their contributions to the final results. A search with a low sensitivity contributes less to the average than searches with higher sensitivity. The overall sensitivity-weighted luminosities at low and high mass are  $5.8 \text{ fb}^{-1}$  and  $6.0 \text{ fb}^{-1}$ , respectively. The Higgs boson decay modes studied are  $H \rightarrow b\bar{b}$ ,  $H \rightarrow W^+W^-$ ,  $H \rightarrow \tau^+\tau^-$  and  $H \rightarrow \gamma\gamma$ .

To simplify the combination, the searches are separated into 129 mutually exclusive final states (56 for CDF and 73 for D0; see Tables II and III) referred to as ‘‘analysis sub-channels’’ in this note. The selection procedures for each analysis are detailed in Refs. [5] through [25], and are briefly described below.

## II. ACCEPTANCE, BACKGROUNDS, AND LUMINOSITY

Event selections are similar for the corresponding CDF and D0 analyses. For the case of  $WH \rightarrow \ell\nu b\bar{b}$ , an isolated lepton ( $\ell =$  electron or muon) and two jets are required, with one or more  $b$ -tagged jets, i.e., identified as containing a weakly-decaying  $B$  hadron. Selected events must also display a significant imbalance in transverse momentum (referred to as missing transverse energy or  $\cancel{E}_T$ ). Events with more than one isolated lepton are vetoed.

For the D0  $WH \rightarrow \ell\nu b\bar{b}$  analyses, the data are split by lepton type and jet multiplicity (two or three jet sub-channels), and in turn for each of these two non-overlapping  $b$ -tagged samples are defined, one being a single ‘‘tight’’  $b$ -tag (ST) sample, and the other a double ‘‘loose’’  $b$ -tag (DT) sample. The tight and loose  $b$ -tagging criteria [26] are defined with respect to the mis-identification rate that the  $b$ -tagging algorithm yields for light quark or gluon jets (‘‘mistag rate’’) typically  $\leq 0.5\%$  or  $\leq 1.5\%$ , respectively. Each sub-channel is analyzed separately. The outputs of random forests, trained separately for each sample and for each Higgs mass, are used as the final discriminating variables in the limit setting procedure.

For the CDF  $WH \rightarrow \ell\nu b\bar{b}$  analyses, events are analyzed in two and three jet sub-channels separately, and in each of these samples the events are grouped into various lepton and  $b$ -tag categories. In addition to the selections requiring an identified lepton, events with an isolated track failing lepton selection requirements in the two jet sample, or an identified loose muon in the extended muon coverage in the three jet sample, are analyzed separately in their own categories. These additional categories provide some acceptance for poorly reconstructed electrons as well as single prong tau decays. Within the lepton categories there are four  $b$ -tagging categories considered in the two jet sample: two tight  $b$ -tags (TDT), one tight  $b$ -tag and one loose  $b$ -tag (LDT), one tight  $b$ -tag and one looser  $b$ -tag (LDTX), and a single, tight,  $b$ -tag (ST). The same  $b$ -tagging categories are used for the three jets channel, although the LDTX category is not used (events with one tight and one looser  $b$ -tags propagate into the one  $b$ -tag category). A Bayesian neural network discriminant is trained at each  $m_H$  in the test range for the two jet sample, separately for each lepton and  $b$ -tagging category, while for the three jet sample a matrix element (ME) discriminant is used.

For the  $ZH \rightarrow \nu\bar{\nu}b\bar{b}$  analyses, the selection is similar to the  $WH$  selection, except all events with isolated leptons are vetoed and stronger multijet background suppression techniques are applied. Both CDF and D0 analyses use a track-based missing transverse momentum calculation as a discriminant against false  $\cancel{E}_T$ . In addition both CDF and D0 utilize multi-variate techniques, a boosted decision tree at D0 and a neural network at CDF, to further discriminate against the multi-jet background before  $b$ -tagging. There is a sizable fraction of the  $WH \rightarrow \ell\nu b\bar{b}$  signal in which the lepton is undetected that is selected in the  $ZH \rightarrow \nu\bar{\nu}b\bar{b}$  samples, so these analyses are also referred to

as  $VH \rightarrow \cancel{E}_T b\bar{b}$ . The CDF analysis uses three non-overlapping categories of  $b$ -tagged events (TDT, LDT and ST as for three jet  $WH \rightarrow \ell\nu b\bar{b}$  channels). D0 uses orthogonal ST and tight-loose double-tag (TLDT) channels. CDF uses neural-network outputs for the final discriminating variables, while D0 uses boosted decision tree outputs. For this combination D0 has updated the TLDT sample to use  $6.4 \text{ fb}^{-1}$  of data and refined the input variables to the decision trees, including, amongst others, event characteristics sensitive to whether the jets originated from a color singlet object.

The  $ZH \rightarrow \ell^+\ell^-b\bar{b}$  analyses require two isolated leptons and at least two jets. D0's  $ZH \rightarrow \ell^+\ell^-b\bar{b}$  analyses separate events into non-overlapping samples of events with one tight  $b$ -tag (ST) and two loose  $b$ -tags (LDT). CDF separates events into single tag (ST), double tag (TDT) and loose double tag (LDT) samples. To increase signal acceptance D0 has loosened the selection criteria for one of the leptons to include an isolated track not reconstructed in the muon detector ( $\mu\mu_{trk}$ ) or an electron from the inter-cryostat region of the D0 detector ( $ee_{ICR}$ ). Combined with the dielectron ( $ee$ ) and dimuon ( $\mu\mu$ ) analyses, these provide four orthogonal analyses, and each uses  $4.2 \text{ fb}^{-1}$  of data. Most recently the  $ee$  and  $\mu\mu$  channels have been updated to include  $6.2 \text{ fb}^{-1}$  of data. CDF has added for this combination additional sub-channels for candidate events with two loose muon candidates selected using a neural network discriminant. Events in the new category are analyzed separately depending on the trigger path (muon or  $\cancel{E}_T$ ) from which they were selected. D0 applies a kinematic to optimize reconstruction. CDF corrects jet energies for  $\cancel{E}_T$  using a neural network approach. For the D0 analysis random forests of decision trees provide the final variables for setting limits, while CDF utilizes outputs of two-dimensional neural networks incorporating likelihoods based on event probabilities obtained from ME calculations as additional inputs.

For the  $H \rightarrow W^+W^-$  analyses, signal events are characterized by large  $\cancel{E}_T$  and two opposite-signed, isolated leptons. The presence of neutrinos in the final state prevents the accurate reconstruction of the candidate Higgs boson mass. D0 selects events containing large  $\cancel{E}_T$  and electrons and/or muons, dividing the data sample into three final states:  $e^+e^-$ ,  $e^\pm\mu^\mp$ , and  $\mu^+\mu^-$ . Final states involving leptonic tau decays and mis-identified hadronic tau decays are included. The  $e^+e^-$  and  $\mu^+\mu^-$  analyses are as in Ref. [21]. The  $e^\pm\mu^\mp$  channel has been updated, and now uses  $6.7 \text{ fb}^{-1}$  of data as well as subdividing the dataset according to the number of jets in the event: 0, 1, or 2+ jets. CDF separates the  $H \rightarrow W^+W^-$  events in five non-overlapping samples, split into both ‘‘high  $s/b$ ’’ and ‘‘low  $s/b$ ’’ categories based on lepton types and different categories based on the number of reconstructed jets: 0, 1, or 2+ jets. The sample with two or more jets is not split into low  $s/b$  and high  $s/b$  lepton categories due to low statistics. A sixth CDF channel is the low dilepton mass ( $m_{\ell^+\ell^-}$ ) channel, which accepts events with  $m_{\ell^+\ell^-} < 16 \text{ GeV}$ . This channel increases the sensitivity of the  $H \rightarrow W^+W^-$  analyses at low  $m_H$ , adding 10% additional acceptance at  $m_H = 120 \text{ GeV}$ .

The division of events into jet categories allows the analysis discriminants to separate three different categories of signals from the backgrounds more effectively. The signal production mechanisms considered are  $gg \rightarrow H \rightarrow W^+W^-$ ,  $WH + ZH \rightarrow jjW^+W^-$ , and vector-boson fusion. For  $gg \rightarrow H$ , recent work [27] indicates that the theoretical uncertainties due to scale and PDF variations are significantly different for the different jet categories. CDF and D0 divide the theoretical uncertainty on  $gg \rightarrow H$  into PDF and scale pieces, and utilize the differential uncertainties of [27]. The D0  $e^+e^-$  and  $\mu^+\mu^-$  channels use neural-network discriminants, including the number of jets as an input, as the final discriminant while the  $e^\pm\mu^\mp$  channel relies on boosted decision tree outputs with additional input variables now included for the 1 and 2+ jet sub-channels. CDF uses neural-network outputs, including likelihoods constructed from calculated ME probabilities as additional inputs for the 0-jet bin.

D0 has updated its  $VH \rightarrow l^\pm l'^\pm + X$  analyses to include additional data and an improved discriminant. The associated vector boson and the  $W$  boson from the Higgs boson decay that has the same charge are required to decay leptonically, thereby defining three like-sign dilepton final states ( $e^\pm e^\pm$ ,  $e^\pm\mu^\pm$ , and  $\mu^\pm\mu^\pm$ ). The combined output of two decision trees, trained against the instrumental and diboson backgrounds respectively, is used as the final discriminant. CDF also includes a separate analysis of events with same-sign leptons and large  $\cancel{E}_T$  to incorporate additional potential signal from associated production events in which the two leptons (one from the associated vector boson and one from a  $W$  boson produced in the Higgs decay) have the same charge. CDF for the first time also incorporates three tri-lepton channels to include additional associated production contributions where leptons result from the associated  $W$  boson and the two  $W$  bosons produced in the Higgs decay or where an associated  $Z$  boson decays into a dilepton pair and a third lepton is produced in the decay of either of the  $W$  bosons resulting from the Higgs decay. In the latter case, CDF separates the sample into 1 jet and 2+ jet sub-channels to fully take advantage of the Higgs mass constraint available in the 2+ jet case where all of the decay products are reconstructed.

For the first time CDF also includes opposite-sign channels in which one of the two lepton candidates is a hadronic

tau. Events are separated into  $e\text{-}\tau$  and  $\mu\text{-}\tau$  channels. The final discriminants are obtained from boosted decision trees which incorporate both hadronic tau identification and kinematic event variables as inputs. Also for the first time D0 includes new channels in which one of the  $W$  bosons in the  $H \rightarrow W^+W^-$  process decays leptonically and the other decays hadronically. Electron and muon final states are studied separately, each with  $5.4 \text{ fb}^{-1}$  of data, with random forests being used for the final discriminants.

CDF contributes an analysis searching for Higgs bosons decaying to a tau lepton pair, in three separate production channels: direct  $gg \rightarrow H$  production, associated  $WH$  or  $ZH$  production, and vector boson production with  $H$  and forward jets in the final state. One or two jets are required in the event selection. In this analysis, the final variable for setting limits is a combination of three boosted signal tree discriminants, each designed to discriminate the signal against one of the major backgrounds (QCD multi-jets,  $Z/\gamma^* \rightarrow \tau^+\tau^-$ , and  $t\bar{t}$ ). The theoretical systematic uncertainty on the  $gg \rightarrow H$  production rate now takes into account recent theoretical work [27] which provides separate uncertainties for each jet category. D0 also contributes an analysis of the  $\tau^+\tau^- + 2$  jets final state, which is sensitive to the  $VH \rightarrow jj\tau^+\tau^-$ ,  $ZH \rightarrow \tau^-\tau^-b\bar{b}$ , VBF and gluon gluon fusion (with two additional jets) production mechanisms. A neural network output is used as the discriminant variable for RunIIa (the first  $1.0 \text{ fb}^{-1}$  of data), while a boosted decision tree output is used for later data.

CDF also includes an updated all-hadronic analysis, which results in two  $b$ -tagging sub-channels (TDT and LDT) for both  $WH/ZH$  and VBF production to the  $jjb\bar{b}$  final state. Events with either four or five reconstructed jets are selected, and at least two must be  $b$ -tagged. The large QCD multi-jet backgrounds are modeled from the data by applying a measured mistag probability to the non  $b$ -tagged jets in events containing a single  $b$ -tag. Neural network discriminants based on kinematic event variables including ones designed to separate quark and gluon jets are used to obtain the final limits.

Both D0 and CDF contribute (CDF for the first time) analyses searching for direct Higgs boson production in which the Higgs decays directly into a pair of photons. These analyses look for a signal peak in the diphoton invariant mass spectrum above the smooth background originating from standard QCD production. Finally, D0 includes the channel  $t\bar{t}H \rightarrow t\bar{t}b\bar{b}$ . Here the samples are analyzed independently according to the number of  $b$ -tagged jets and the total number of jets. The scalar sum of the transverse energies of the reconstructed objects ( $H_T$ ) is used as the discriminant variable.

We normalize our Higgs boson signal predictions to the most recent high-order calculations available. The  $gg \rightarrow H$  production cross section is calculated at NNLL in QCD and also includes two-loop electroweak effects, and handling of the running  $b$  quark mass [28, 29]. These calculations are refinements of the earlier NNLO calculations of the  $gg \rightarrow H$  production cross section [30–32]. Electroweak corrections were computed in Refs. [33, 34]. Soft gluon resummation was introduced in the prediction of the  $gg \rightarrow H$  production cross section in Ref. [35].

The  $gg \rightarrow H$  production cross section depends strongly on the gluon parton density function, and the accompanying value of  $\alpha_s(q^2)$ . The cross sections used here are calculated with the MSTW 2008 NNLO PDF set [36]. The Higgs boson production cross sections are listed in Table I. We include the larger theoretical uncertainties due to scale variations and PDF variations separately for each jet bin for the  $gg \rightarrow H$  processes as evaluated in Ref. [27]. We treat the scale uncertainties as 100% correlated between jet bins and between CDF and D0, and also treat the PDF uncertainties in the cross section as correlated between jet bins and between CDF and D0.

We include all significant Higgs production modes in the high-mass search. Besides gluon-gluon fusion through virtual quark loops (ggH), we include Higgs boson production in association with a  $W$  or  $Z$  vector boson (VH) [37–39], and vector boson fusion (VBF) [37, 40]. For the low-mass searches, we target the  $WH$ ,  $ZH$ , VBF, and  $t\bar{t}H$  [41] production modes with specific searches, including also those signal components not specifically targeted but which fall in the acceptance nonetheless. Our  $WH$  and  $ZH$  cross sections are from Ref. [42]. We include the  $ggH$  production mode in our searches for Higgs bosons decaying to tau pairs and photon pairs. In order to predict the distributions of the kinematics of Higgs boson signal events, CDF and D0 use the PYTHIA [43] Monte Carlo program, with CTEQ5L and CTEQ6L [44] leading-order (LO) parton distribution functions. The Higgs boson decay branching ratio predictions are calculated with HDECAY [45], and are also listed in Table I. We use HDECAY Version 3.53.

For both CDF and D0, events from QCD multijet (instrumental) backgrounds are measured in independent data samples using several different methods. For CDF, backgrounds from SM processes with electroweak gauge bosons or top quarks were generated using PYTHIA, ALPGEN [46], MC@NLO [47], and HERWIG [48] programs. For D0, these backgrounds were generated using PYTHIA, ALPGEN, and COMPHEP [49], with PYTHIA providing parton-showering and hadronization for all the generators. These background processes were normalized using either

experimental data or next-to-leading order calculations (including MCFM [50] for the  $W$  + heavy flavor process).

Tables II and III summarize, for CDF and D0 respectively, the integrated luminosities, the Higgs boson mass ranges over which the searches are performed, and references to further details for each analysis.

### III. DISTRIBUTIONS OF CANDIDATES

All analyses provide binned histograms of the final discriminant variables for the signal and background predictions, itemized separately for each source, and the observed data. The number of channels combined is large, and the number of bins in each channel is large. Therefore, the task of assembling histograms and checking whether the expected and observed limits are consistent with the input predictions and observed data is difficult. We therefore provide histograms that aggregate all channels' signal, background, and data together. In order to preserve most of the sensitivity gain that is achieved by the analyses by binning the data instead of collecting them all together and counting, we aggregate the data and predictions in narrow bins of signal-to-background ratio,  $s/b$ . Data with similar  $s/b$  may be added together with no loss in sensitivity, assuming similar systematic errors on the predictions. The aggregate histograms do not show the effects of systematic uncertainties, but instead compare the data with the central predictions supplied by each analysis.

The range of  $s/b$  is quite large in each analysis, and so  $\log_{10}(s/b)$  is chosen as the plotting variable. Plots of the distributions of  $\log_{10}(s/b)$  are shown for Higgs boson masses of 100, 115, 150, and 165  $\text{GeV}/c^2$  in Figure 1. These distributions can be integrated from the high- $s/b$  side downwards, showing the sums of signal, background, and data for the most pure portions of the selection of all channels added together. These integrals can be seen in Figure 2. The most significant candidates are found in the bins with the highest  $s/b$ ; an excess in these bins relative to the background prediction drives the Higgs boson cross section limit upwards, while a deficit drives it downwards. The lower- $s/b$  bins show that the modeling of the rates and kinematic distributions of the backgrounds is very good. The integrated plots show the excess of events in the highest- $s/b$  bins for the analyses seeking a Higgs boson mass of 115  $\text{GeV}/c^2$ , and a deficit of events in the highest- $s/b$  bins for the analyses seeking a Higgs boson of mass 165  $\text{GeV}/c^2$ .

We also show the distributions of the data after subtracting the expected background, and compare that with the expected signal yield for a Standard Model Higgs boson, after collecting all bins in all channels sorted by  $s/b$ . These background-subtracted distributions are shown in Figure 3. These graphs also show the remaining uncertainty on the background prediction after fitting the background model to the data within the systematic uncertainties on the rates and shapes in each contributing channel's templates.

### IV. COMBINING CHANNELS

To gain confidence that the final result does not depend on the details of the statistical formulation, we perform two types of combinations, using Bayesian and Modified Frequentist approaches, which yield limits on the Higgs boson production rate that agree within 10% at each value of  $m_H$ , and within 1% on average. Both methods rely on distributions in the final discriminants, and not just on their single integrated values. Systematic uncertainties enter on the predicted number of signal and background events as well as on the distribution of the discriminants in each analysis ("shape uncertainties"). Both methods use likelihood calculations based on Poisson probabilities.

#### A. Bayesian Method

Because there is no experimental information on the production cross section for the Higgs boson, in the Bayesian technique [1] we assign a flat prior for the total number of selected Higgs events. For a given Higgs boson mass, the combined likelihood is a product of likelihoods for the individual channels, each of which is a product over histogram bins:

TABLE I: The production cross sections and decay branching fractions for the SM Higgs boson assumed for the combination.

$m_H$ (GeV/ $c^2$ )	$\sigma_{gg \rightarrow H}$ (fb)	$\sigma_{WH}$ (fb)	$\sigma_{ZH}$ (fb)	$\sigma_{VBF}$ (fb)	$\sigma_{t\bar{t}H}$ (fb)	$B(H \rightarrow b\bar{b})$ (%)	$B(H \rightarrow c\bar{c})$ (%)	$B(H \rightarrow \tau^+\tau^-)$ (%)	$B(H \rightarrow W^+W^-)$ (%)	$B(H \rightarrow ZZ)$ (%)	$B(H \rightarrow \gamma\gamma)$ (%)
100	1861	291.9	169.8	99.5	8.000	80.33	3.542	7.920	1.052	0.1071	0.1505
105	1618	248.4	145.9	93.3	7.062	78.57	3.463	7.821	2.307	0.2035	0.1689
110	1413	212.0	125.7	87.1	6.233	75.90	3.343	7.622	4.585	0.4160	0.1870
115	1240	181.9	108.9	79.07	5.502	71.95	3.169	7.288	8.268	0.8298	0.2029
120	1093	156.4	94.4	71.65	4.857	66.49	2.927	6.789	13.64	1.527	0.2148
125	967	135.1	82.3	67.37	4.279	59.48	2.617	6.120	20.78	2.549	0.2204
130	858	116.9	71.9	62.5	3.769	51.18	2.252	5.305	29.43	3.858	0.2182
135	764	101.5	63.0	57.65	3.320	42.15	1.854	4.400	39.10	5.319	0.2077
140	682	88.3	55.3	52.59	2.925	33.04	1.453	3.472	49.16	6.715	0.1897
145	611	77.0	48.7	49.15	2.593	24.45	1.075	2.585	59.15	7.771	0.1653
150	548	67.3	42.9	45.67	2.298	16.71	0.7345	1.778	68.91	8.143	0.1357
155	492	58.9	37.9	42.19	2.037	9.88	0.4341	1.057	78.92	7.297	0.09997
160	439	50.8	33.1	38.59	1.806	3.74	0.1646	0.403	90.48	4.185	0.05365
165	389	44.6	30.0	36.09	1.607	1.29	0.05667	0.140	95.91	2.216	0.02330
170	349	40.2	26.6	33.58	1.430	0.854	0.03753	0.093	96.39	2.351	0.01598
175	314	35.6	23.7	31.11	1.272	0.663	0.02910	0.073	95.81	3.204	0.01236
180	283	31.4	21.1	28.57	1.132	0.535	0.02349	0.059	93.25	5.937	0.01024
185	255	28.2	18.9	26.81	1.004	0.415	0.01823	0.046	84.50	14.86	0.008128
190	231	25.1	17.0	24.88	0.890	0.340	0.01490	0.038	78.70	20.77	0.006774
195	210	22.4	15.3	23	0.789	0.292	0.01281	0.033	75.88	23.66	0.005919
200	192	20.0	13.7	21.19	0.700	0.257	0.01128	0.029	74.26	25.33	0.005285

TABLE II: Luminosity, explored mass range and references for the different processes and final states ( $\ell = e, \mu$ ) for the CDF analyses. The labels “2 $\times$ ” and “4 $\times$ ” refer to separation into different lepton categories.

Channel	Luminosity (fb <sup>-1</sup> )	$m_H$ range (GeV/ $c^2$ )	Reference
$WH \rightarrow \ell\nu b\bar{b}$ 2-jet channels	4 $\times$ (TDT,LDT,ST,LDTX)	5.7	100-150 [5]
$WH \rightarrow \ell\nu b\bar{b}$ 3-jet channels	2 $\times$ (TDT,LDT,ST)	5.6	100-150 [6]
$ZH \rightarrow \nu\bar{\nu} b\bar{b}$	(TDT,LDT,ST)	5.7	100-150 [7]
$ZH \rightarrow \ell^+\ell^- b\bar{b}$	4 $\times$ (TDT,LDT,ST)	5.7	100-150 [8, 9]
$H \rightarrow W^+W^-$	2 $\times$ (0,1 jets)+(2+ jets)+(low- $m_{\ell\ell}$ )+(e- $\tau_{had}$ )+( $\mu$ - $\tau_{had}$ )	5.9	110-200 [10]
$WH \rightarrow WW^+W^-$	(same-sign leptons 1+ jets)+(tri-leptons)	5.9	110-200 [10]
$ZH \rightarrow ZW^+W^-$	(tri-leptons 1 jet)+(tri-leptons 2+ jets)	5.9	110-200 [10]
$H + X \rightarrow \tau^+\tau^-$	(1 jet)+(2 jets)	2.3	100-150 [11]
$WH + ZH \rightarrow jj b\bar{b}$	2 $\times$ (TDT,LDT)	4.0	100-150 [12]
$H \rightarrow \gamma\gamma$		5.4	100-150 [13]

TABLE III: Luminosity, explored mass range and references for the different processes and final states ( $\ell = e, \mu$ ) for the D0 analyses. Most analyses are in addition analyzed separately for RunIIa and IIb. In some cases, not every sub-channel uses the same dataset, and a range of integrated luminosities is given.

Channel	Luminosity (fb <sup>-1</sup> )	$m_H$ range (GeV/ $c^2$ )	Reference
$WH \rightarrow \ell\nu b\bar{b}$	(ST,DT,2,3 jet)	5.3	100-150 [14]
$VH \rightarrow \tau^+\tau^- b\bar{b}/q\bar{q}\tau^+\tau^-$		4.9	105-145 [15, 16]
$ZH \rightarrow \nu\bar{\nu} b\bar{b}$	(ST,TLDT)	5.2-6.4	100-150 [17, 18]
$ZH \rightarrow \ell^+\ell^- b\bar{b}$	(ST,DT,ee, $\mu\mu$ ,eeICR, $\mu\mu_{trk}$ )	4.2-6.2	100-150 [19]
$VH \rightarrow \ell^\pm\ell^\pm + X$		5.3	115-200 [20]
$H \rightarrow W^+W^- \rightarrow e^\pm\nu e^\mp\nu, \mu^\pm\nu\mu^\mp\nu$		5.4	115-200 [21]
$H \rightarrow W^+W^- \rightarrow e^\pm\nu\mu^\mp\nu$	(0,1,2+ jet)	6.7	115-200 [22]
$H \rightarrow W^+W^- \rightarrow \ell\bar{\nu}jj$		5.4	130-200 [23]
$H \rightarrow \gamma\gamma$		4.2	100-150 [24]
$t\bar{t}H \rightarrow t\bar{t} b\bar{b}$	(ST,DT,TT,4,5+ jets)	2.1	105-155 [25]

$$\mathcal{L}(R, \vec{s}, \vec{b}|\vec{n}, \vec{\theta}) \times \pi(\vec{\theta}) = \prod_{i=1}^{N_C} \prod_{j=1}^{N_b} \mu_{ij}^{n_{ij}} e^{-\mu_{ij}} / n_{ij}! \times \prod_{k=1}^{n_p} e^{-\theta_k^2/2} \quad (1)$$

where the first product is over the number of channels ( $N_C$ ), and the second product is over  $N_b$  histogram bins containing  $n_{ij}$  events, binned in ranges of the final discriminants used for individual analyses, such as the dijet mass, neural-network outputs, or matrix-element likelihoods. The parameters that contribute to the expected bin contents are  $\mu_{ij} = R \times s_{ij}(\vec{\theta}) + b_{ij}(\vec{\theta})$  for the channel  $i$  and the histogram bin  $j$ , where  $s_{ij}$  and  $b_{ij}$  represent the expected background and signal in the bin, and  $R$  is a scaling factor applied to the signal to test the sensitivity level of the experiment. Truncated Gaussian priors are used for each of the nuisance parameters  $\theta_k$ , which define the sensitivity of the predicted signal and background estimates to systematic uncertainties. These can take the form of uncertainties on overall rates, as well as the shapes of the distributions used for combination. These systematic uncertainties can be far larger than the expected SM Higgs boson signal, and are therefore important in the calculation of limits. The truncation is applied so that no prediction of any signal or background in any bin is negative. The posterior density function is then integrated over all parameters (including correlations) except for  $R$ , and a 95% credibility level upper limit on  $R$  is estimated by calculating the value of  $R$  that corresponds to 95% of the area of the resulting distribution.

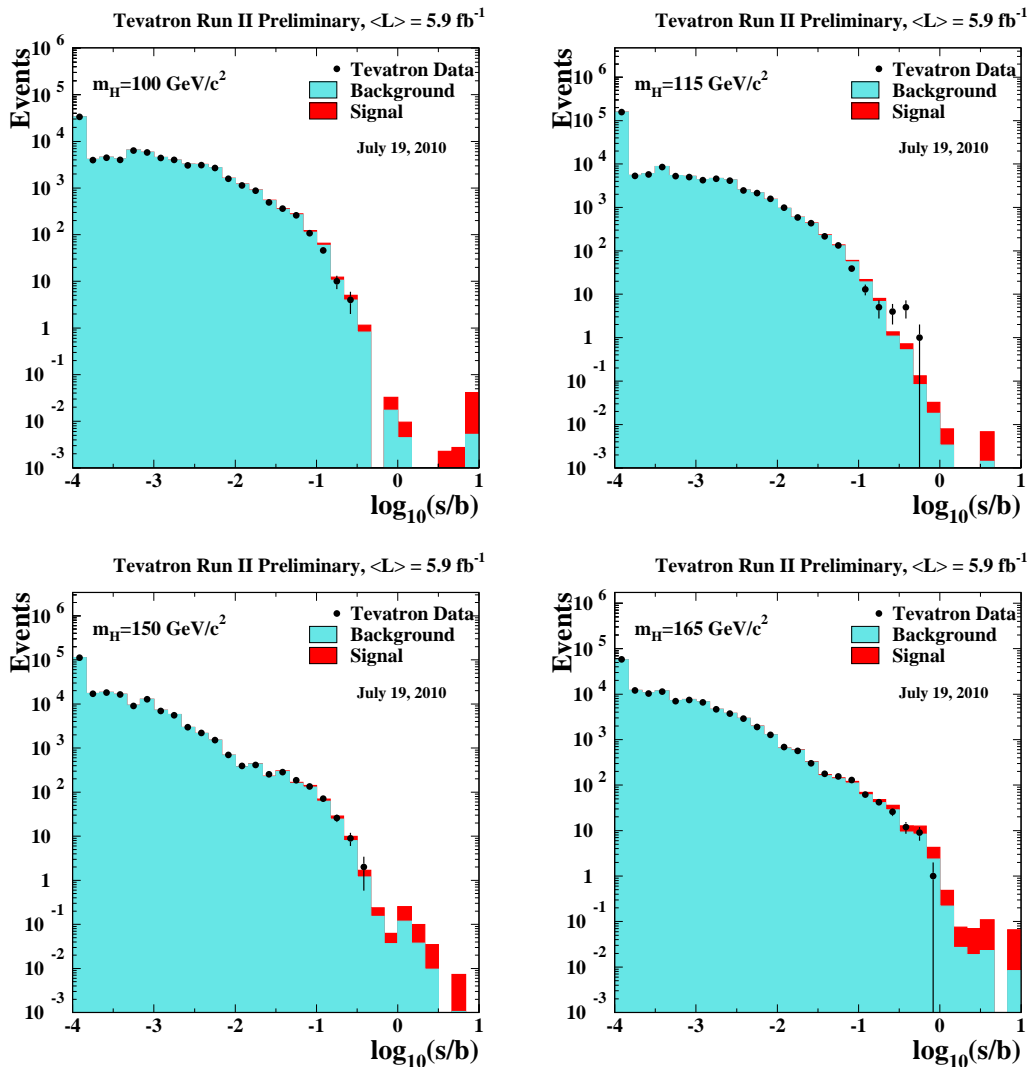


FIG. 1: Distributions of  $\log_{10}(s/b)$ , for the data from all contributing channels from CDF and D0, for Higgs boson masses of 100, 115, 150, and 165  $\text{GeV}/c^2$ . The data are shown with points, and the expected signal is shown stacked on top of the backgrounds. Underflows and overflows are collected into the bottom and top bins.

## B. Modified Frequentist Method

The Modified Frequentist technique relies on the  $\text{CL}_s$  method, using a log-likelihood ratio (LLR) as test statistic [2]:

$$LLR = -2 \ln \frac{p(\text{data}|H_1)}{p(\text{data}|H_0)}, \quad (2)$$

where  $H_1$  denotes the test hypothesis, which admits the presence of SM backgrounds and a Higgs boson signal, while  $H_0$  is the null hypothesis, for only SM backgrounds. The probabilities  $p$  are computed using the best-fit values of the nuisance parameters for each pseudo-experiment, separately for each of the two hypotheses, and include the Poisson probabilities of observing the data multiplied by Gaussian priors for the values of the nuisance parameters. This



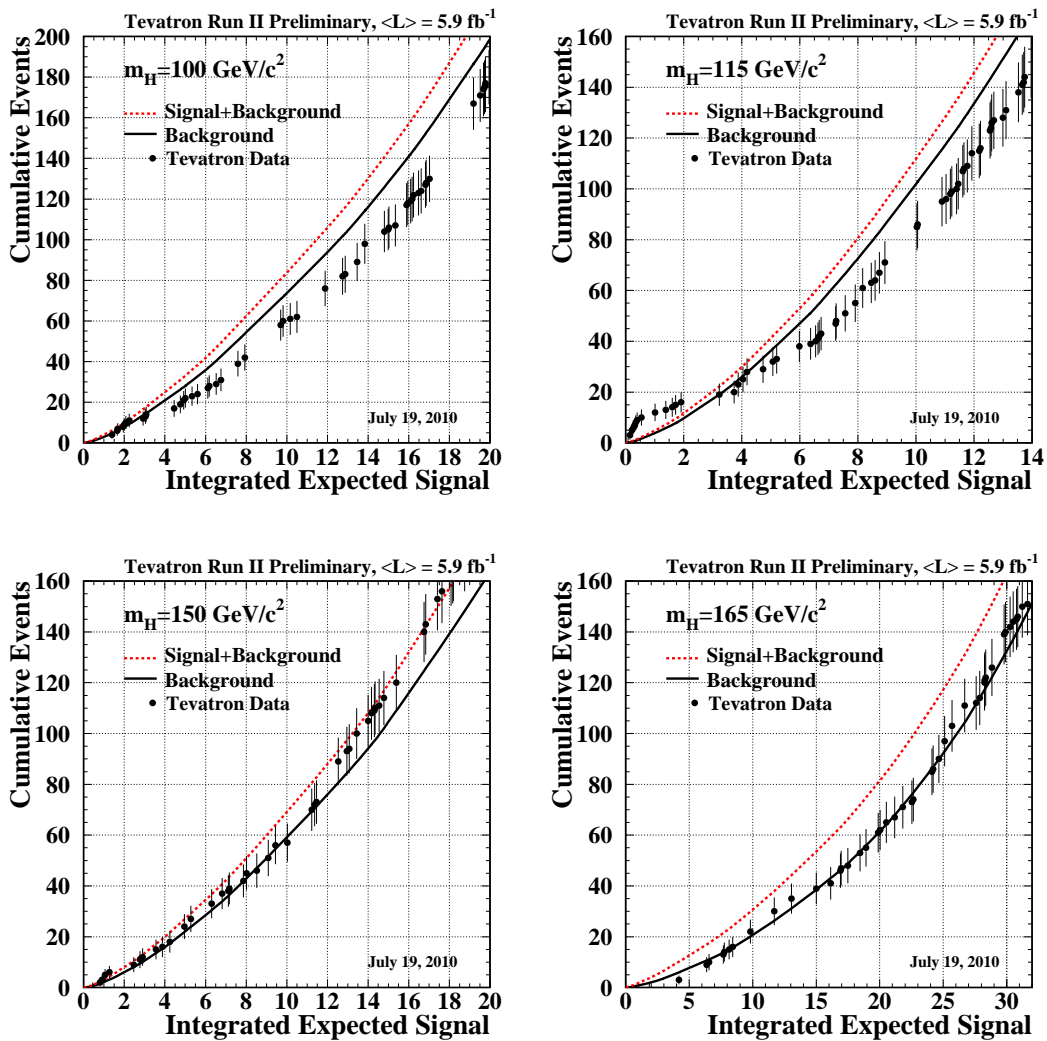


FIG. 2: Integrated distributions of  $s/b$ , starting at the high  $s/b$  side, for Higgs boson masses of 100, 115, 150, and 165  $\text{GeV}/c^2$ . The total signal+background and background-only integrals are shown separately, along with the data sums. Data are only shown for bins that have data events in them.

technique extends the LEP procedure [51] which does not involve a fit, in order to yield better sensitivity when expected signals are small and systematic uncertainties on backgrounds are large [52].

The  $\text{CL}_s$  technique involves computing two  $p$ -values,  $\text{CL}_{s+b}$  and  $\text{CL}_b$ . The latter is defined by

$$1 - \text{CL}_b = p(LLR \leq LLR_{\text{obs}} | H_0), \quad (3)$$

where  $LLR_{\text{obs}}$  is the value of the test statistic computed for the data.  $1 - \text{CL}_b$  is the probability of observing a signal-plus-background-like outcome without the presence of signal, i.e. the probability that an upward fluctuation of the background provides a signal-plus-background-like response as observed in data. The other  $p$ -value is defined by

$$\text{CL}_{s+b} = p(LLR \geq LLR_{\text{obs}} | H_1), \quad (4)$$

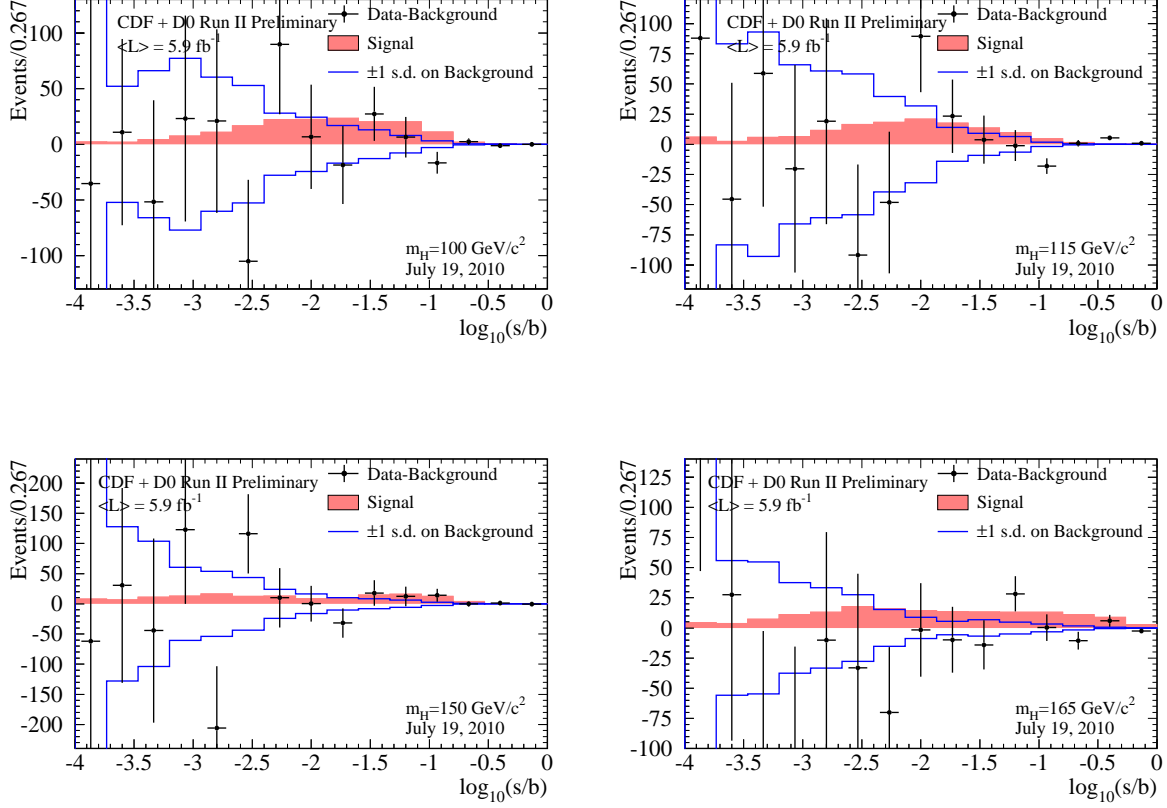


FIG. 3: Background-subtracted data distributions for all channels, summed in bins of  $s/b$ , for Higgs boson masses of 100, 115, 150, and 165  $\text{GeV}/c^2$ . The background has been fit, within its systematic uncertainties, to the data. The points with error bars indicate the background-subtracted data; the sizes of the error bars are the square roots of the predicted background in each bin. The unshaded (blue-outline) histogram shows the systematic uncertainty on the best-fit background model, and the shaded histogram shows the expected signal for a Standard Model Higgs boson.

and this corresponds to the probability of a downward fluctuation of the sum of signal and background in the data. A small value of  $\text{CL}_{s+b}$  reflects inconsistency with  $H_1$ . It is also possible to have a downward fluctuation in data even in the absence of any signal, and a small value of  $\text{CL}_{s+b}$  is possible even if the expected signal is so small that it cannot be tested with the experiment. To minimize the possibility of excluding a signal to which there is insufficient sensitivity (an outcome expected 5% of the time at the 95% C.L., for full coverage), we use the quantity  $\text{CL}_s = \text{CL}_{s+b}/\text{CL}_b$ . If  $\text{CL}_s < 0.05$  for a particular choice of  $H_1$ , that hypothesis is deemed to be excluded at the 95% C.L. In an analogous way, the expected  $\text{CL}_b$ ,  $\text{CL}_{s+b}$  and  $\text{CL}_s$  values are computed from the median of the LLR distribution for the background-only hypothesis.

Systematic uncertainties are included by fluctuating the predictions for signal and background rates in each bin of each histogram in a correlated way when generating the pseudo-experiments used to compute  $\text{CL}_{s+b}$  and  $\text{CL}_b$ .

### C. Systematic Uncertainties

Systematic uncertainties differ between experiments and analyses, and they affect the rates and shapes of the predicted signal and background in correlated ways. The combined results incorporate the sensitivity of predictions to values of nuisance parameters, and include correlations between rates and shapes, between signals and backgrounds, and between channels within experiments and between experiments. More on these issues can be found in the individual analysis notes [5] through [25]. Here we consider only the largest contributions and correlations between and within the two experiments.

#### 1. Correlated Systematics between CDF and D0

The uncertainties on the measurements of the integrated luminosities are 6% (CDF) and 6.1% (D0). Of these values, 4% arises from the uncertainty on the inelastic  $p\bar{p}$  scattering cross section, which is correlated between CDF and D0. CDF and D0 also share the assumed values and uncertainties on the production cross sections for top-quark processes ( $t\bar{t}$  and single top) and for electroweak processes ( $WW$ ,  $WZ$ , and  $ZZ$ ). In order to provide a consistent combination, the values of these cross sections assumed in each analysis are brought into agreement. We use  $\sigma_{t\bar{t}} = 7.04_{-0.36}^{+0.24}$  (scale)  $\pm 0.14$ (PDF)  $\pm 0.30$ (mass), following the calculation of Moch and Uwer [53], assuming a top quark mass  $m_t = 173.0 \pm 1.2$  GeV/ $c^2$  [54], and using the MSTW2008nnlo PDF set [36]. Other calculations of  $\sigma_{t\bar{t}}$  are similar [55].

For single top, we use the NLL  $t$ -channel calculation of Kidonakis [56], which has been updated using the MSTW2008nnlo PDF set [36] [57]. For the  $s$ -channel process we use [58], again based on the MSTW2008nnlo PDF set. Both of the cross section values below are the sum of the single  $t$  and single  $\bar{t}$  cross sections, and both assume  $m_t = 173 \pm 1.2$  GeV.

$$\sigma_{t\text{-chan}} = 2.10 \pm 0.027(\text{scale}) \pm 0.18(\text{PDF}) \pm 0.045(\text{mass})\text{pb.} \quad (5)$$

$$\sigma_{s\text{-chan}} = 1.046 \pm 0.006(\text{scale}) \pm 0.059 (\text{PDF}) \pm 0.030 (\text{mass}) \text{ pb.} \quad (6)$$

Other calculations of  $\sigma_{\text{SingleTop}}$  are similar for our purposes [59].

MCFM [50] has been used to compute the NLO cross sections for  $WW$ ,  $WZ$ , and  $ZZ$  production [60]. Using a scale choice  $\mu_0 = M_V^2 + p_T^2(V)$  and the MSTW2008 PDF set [36], the cross section for inclusive  $W^+W^-$  production is

$$\sigma_{W^+W^-} = 11.34_{-0.49}^{+0.56} (\text{scale})_{-0.28}^{+0.35}(\text{PDF})\text{pb} \quad (7)$$

and the cross section for inclusive  $W^\pm Z$  production is

$$\sigma_{W^\pm Z} = 3.22_{-0.17}^{+0.20} (\text{scale})_{-0.08}^{+0.11} (\text{PDF}) \text{ pb} \quad (8)$$

For the  $Z$ , leptonic decays are used in the definition, with both  $\gamma$  and  $Z$  exchange. The cross section quoted above involves the requirement  $75 \leq m_{\ell+\ell-} \leq 105$  GeV for the leptons from the neutral current exchange. The same dilepton invariant mass requirement is applied to both sets of leptons in determining the  $ZZ$  cross section which is

$$\sigma_{ZZ} = 1.20_{-0.04}^{+0.05} (\text{scale})_{-0.03}^{+0.04} (\text{PDF}) \text{ pb} \quad (9)$$

For the diboson cross section calculations,  $|\eta_\ell| < 5$  for all calculations. Loosening this requirement to include all leptons leads to  $\sim +0.4\%$  change in the predictions. Lowering the factorization and renormalization scales by a factor of two increases the cross section, and raising the scales by a factor of two decreases the cross section. The PDF uncertainty has the same fractional impact on the predicted cross section independent of the scale choice. All PDF uncertainties are computed as the quadrature sum of the twenty 68% C.L. eigenvectors provided with MSTW2008 (MSTW2008nlo68cl).

In many analyses, the dominant background yields are calibrated with data control samples. Since the methods of measuring the multijet (“QCD”) backgrounds differ between CDF and D0, and even between analyses within

the collaborations, there is no correlation assumed between these rates. Similarly, the large uncertainties on the background rates for  $W$ +heavy flavor (HF) and  $Z$ +heavy flavor are considered at this time to be uncorrelated, as both CDF and D0 estimate these rates using data control samples, but employ different techniques. The calibrations of fake leptons, unvetoes  $\gamma \rightarrow e^+e^-$  conversions,  $b$ -tag efficiencies and mistag rates are performed by each collaboration using independent data samples and methods, and are therefore also treated as uncorrelated.

### 2. Correlated Systematic Uncertainties for CDF

The dominant systematic uncertainties for the CDF analyses are shown in the Appendix in Tables VIII and IX for the  $WH \rightarrow \ell\nu b\bar{b}$  channels, in Table XI for the  $WH, ZH \rightarrow \cancel{E}_T b\bar{b}$  channels, in Tables XIII and XIV for the  $ZH \rightarrow \ell^+\ell^- b\bar{b}$  channels, in Tables XVI, XVII, and XVIII for the  $H \rightarrow W^+W^- \rightarrow \ell'^{\pm}\nu\ell'^{\mp}\nu$  channels, in Table XIX for the  $WH \rightarrow WWW \rightarrow \ell'^{\pm}\ell'^{\pm}$  and  $WH \rightarrow WWW \rightarrow \ell^{\pm}\ell'^{\pm}\ell''^{\mp}$  channels, in Table XX for the  $ZH \rightarrow ZWW \rightarrow \ell^{\pm}\ell'^{\mp}\ell'^{\pm}$  channels, in Table XXV for the  $H \rightarrow \tau^+\tau^-$  channels, in Table XXVI for the  $WH/ZH$  and VBF  $\rightarrow jjb\bar{b}$  channels, and in Table XXVII for the  $H \rightarrow \gamma\gamma$  channel. Each source induces a correlated uncertainty across all CDF channels' signal and background contributions which are sensitive to that source. For  $H \rightarrow b\bar{b}$ , the largest uncertainties on signal arise from measured  $b$ -tagging efficiencies, jet energy scale, and other Monte Carlo modeling. Shape dependencies of templates on jet energy scale,  $b$ -tagging, and gluon radiation (“ISR” and “FSR”) are taken into account for some analyses (see tables). For  $H \rightarrow W^+W^-$ , the largest uncertainties on signal acceptance originate from Monte Carlo modeling. Uncertainties on background event rates vary significantly for the different processes. The backgrounds with the largest systematic uncertainties are in general quite small. Such uncertainties are constrained by fits to the nuisance parameters, and they do not affect the result significantly. Because the largest background contributions are measured using data, these uncertainties are treated as uncorrelated for the  $H \rightarrow b\bar{b}$  channels. The differences in the resulting limits when treating the remaining uncertainties as either correlated or uncorrelated, is less than 5%.

### 3. Correlated Systematic Uncertainties for D0

The dominant systematic uncertainties for the D0 analyses are shown in the Appendix, in Tables X, XII, XV, XXI, XXII, XXIII, XXIV, and XXVIII. Each source induces a correlated uncertainty across all D0 channels sensitive to that source. Wherever appropriate the impact of systematic effects on both the rate and shape of the predicted signal and background is included. For the low mass,  $H \rightarrow b\bar{b}$  analyses, the largest sources of uncertainty originate from the measured  $b$ -tagging rate, the determination of the jet energy scale, simulated acceptances, jet resolution, normalization of the  $W$  and  $Z$  plus heavy flavor backgrounds, and determination of the multijet background contribution. For the  $H \rightarrow W^+W^-$  and  $VH \rightarrow l^{\pm}l'^{\pm} + X$  analyses, a significant source of uncertainty is the measured efficiencies for selecting leptons. Significant sources for all analyses are the uncertainties on the luminosity and the cross sections for the simulated backgrounds. All systematic uncertainties arising from the same source are taken to be correlated among the different backgrounds and between signal and background.

## V. COMBINED RESULTS

Before extracting the combined limits we study the distributions of the log-likelihood ratio (LLR) for different hypotheses, to quantify the expected sensitivity across the mass range tested. Figure 4 displays the LLR distributions for the combined analyses as functions of  $m_H$ . Included are the median of the LLR distributions for the background-only hypothesis ( $\text{LLR}_b$ ), the signal-plus-background hypothesis ( $\text{LLR}_{s+b}$ ), and the observed value for the data ( $\text{LLR}_{\text{obs}}$ ). The shaded bands represent the one and two standard deviation ( $\sigma$ ) departures for  $\text{LLR}_b$  centered on the median. Table IV lists the observed and expected LLR values shown in Figure 4.

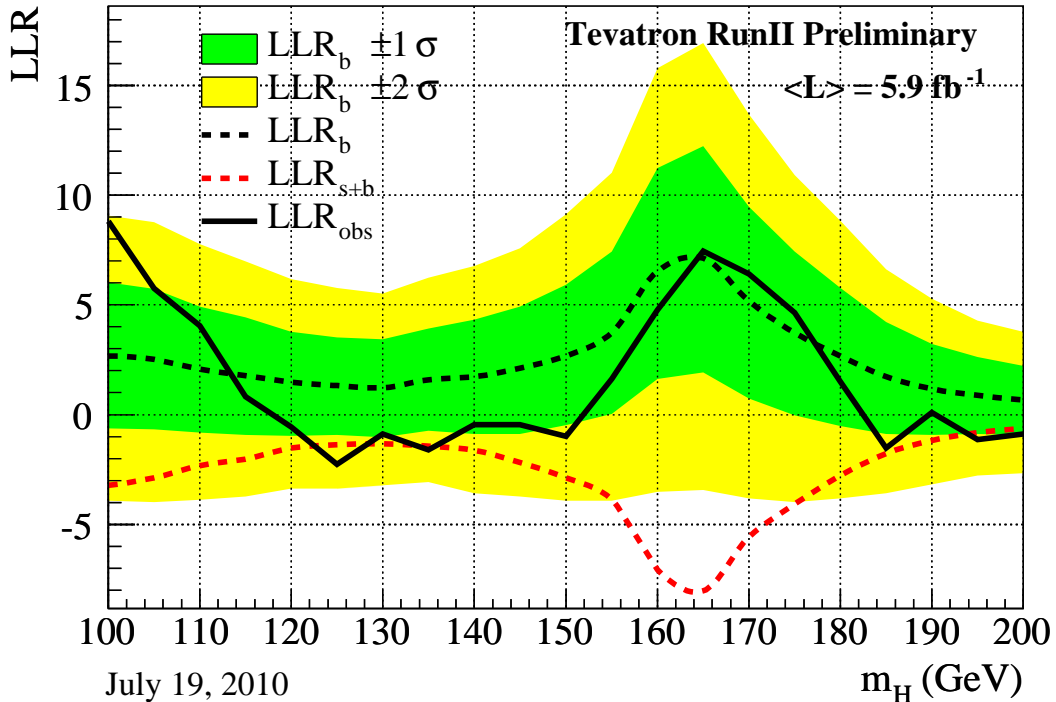


FIG. 4: Distributions of the log-likelihood ratio (LLR) as a function of Higgs mass obtained with the  $CL_s$  method for the combination of all CDF and D0 analyses.

These distributions can be interpreted as follows: The separation between the medians of the  $LLR_b$  and  $LLR_{s+b}$  distributions provides a measure of the discriminating power of the search. The sizes of the one- and two- $\sigma$   $LLR_b$  bands indicate the width of the  $LLR_b$  distribution, assuming no signal is truly present and only statistical fluctuations and systematic effects are present. The value of  $LLR_{obs}$  relative to  $LLR_{s+b}$  and  $LLR_b$  indicates whether the data distribution appears to resemble what we expect if a signal is present (i.e. closer to the  $LLR_{s+b}$  distribution, which is negative by construction) or whether it resembles the background expectation more closely; the significance of any departures of  $LLR_{obs}$  from  $LLR_b$  can be evaluated by the width of the  $LLR_b$  bands.

Using the combination procedures outlined in Section III, we extract limits on SM Higgs boson production  $\sigma \times B(H \rightarrow X)$  in  $p\bar{p}$  collisions at  $\sqrt{s} = 1.96$  TeV for  $100 \leq m_H \leq 200$  GeV/ $c^2$ . To facilitate comparisons with the standard model and to accommodate analyses with different degrees of sensitivity, we present our results in terms of the ratio of obtained limits to the SM Higgs boson production cross section, as a function of Higgs boson mass, for test masses for which both experiments have performed dedicated searches in different channels. A value of the combined limit ratio which is less than or equal to one indicates that that particular Higgs boson mass is excluded at the 95% C.L.

The combinations of results [1, 2] of each single experiment, as used in this Tevatron combination, yield the following ratios of 95% C.L. observed (expected) limits to the SM cross section: 1.79 (1.90) for CDF and 2.52 (2.36) for D0 at  $m_H = 115$  GeV/ $c^2$ , and 1.13 (1.00) for CDF and 1.02 (1.14) for D0 at  $m_H = 165$  GeV/ $c^2$ .

The ratios of the 95% C.L. expected and observed limit to the SM cross section are shown in Figure 5 for the combined CDF and D0 analyses. The observed and median expected ratios are listed for the tested Higgs boson masses in Table V for  $m_H \leq 150$  GeV/ $c^2$ , and in Table VI for  $m_H \geq 155$  GeV/ $c^2$ , as obtained by the Bayesian and the  $CL_s$  methods. In the following summary we quote only the limits obtained with the Bayesian method, which was decided upon *a priori*. It turns out that the Bayesian limits are slightly less stringent. The corresponding limits and expected limits obtained using the  $CL_s$  method are shown alongside the Bayesian limits in the tables. We obtain

TABLE IV: Log-likelihood ratio (LLR) values for the combined CDF + D0 Higgs boson search obtained using the CL<sub>S</sub> method.

$m_H$ (GeV/ $c^2$ )	LLR <sub>obs</sub>	LLR <sub>S+B</sub> <sup>med</sup>	LLR <sub>B</sub> <sup>-2σ</sup>	LLR <sub>B</sub> <sup>-1σ</sup>	LLR <sub>B</sub> <sup>med</sup>	LLR <sub>B</sub> <sup>+1σ</sup>	LLR <sub>B</sub> <sup>+2σ</sup>
100	8.81	-3.23	9.07	6.03	2.67	-0.62	-3.92
105	5.75	-2.88	8.78	5.72	2.52	-0.68	-3.98
110	4.06	-2.33	7.78	4.92	2.08	-0.82	-3.88
115	0.83	-2.02	6.97	4.42	1.77	-0.93	-3.73
120	-0.56	-1.52	6.17	3.77	1.48	-0.97	-3.38
125	-2.26	-1.38	5.78	3.52	1.32	-0.93	-3.38
130	-0.87	-1.32	5.53	3.42	1.23	-1.02	-3.23
135	-1.61	-1.44	6.24	3.91	1.59	-0.74	-3.06
140	-0.45	-1.62	6.78	4.33	1.73	-0.88	-3.58
145	-0.45	-2.17	7.58	4.92	2.12	-0.88	-3.73
150	-0.99	-2.88	9.12	5.92	2.67	-0.47	-3.92
155	1.63	-3.88	11.03	7.42	3.73	0.03	-3.92
160	4.78	-7.08	15.78	11.22	6.53	1.62	-3.52
165	7.46	-8.03	16.93	12.22	7.12	1.93	-3.42
170	6.41	-5.58	13.68	9.47	5.17	0.72	-3.83
175	4.64	-4.08	10.93	7.42	3.73	-0.03	-3.98
180	1.50	-2.77	8.82	5.78	2.67	-0.53	-3.83
185	-1.52	-1.77	6.62	4.22	1.73	-0.88	-3.58
190	0.09	-1.18	5.28	3.23	1.18	-0.93	-3.17
195	-1.13	-0.82	4.28	2.62	0.88	-0.88	-2.77
200	-0.89	-0.62	3.77	2.23	0.68	-0.93	-2.67

the observed (expected) values of 0.87 (1.24) at  $m_H = 105$  GeV/ $c^2$ , 1.56 (1.45) at  $m_H = 115$  GeV/ $c^2$ , 1.28 (1.07) at  $m_H = 155$  GeV/ $c^2$ , 0.68 (0.76) at  $m_H = 165$  GeV/ $c^2$ , 0.95 (1.04) at  $m_H = 175$  GeV/ $c^2$  and 2.55 (1.61) at  $m_H = 185$  GeV/ $c^2$ .

TABLE V: Ratios of median expected and observed 95% C.L. limit to the SM cross section for the combined CDF and D0 analyses as a function of the Higgs boson mass in GeV/ $c^2$ , obtained with the Bayesian and with the CL<sub>S</sub> method.

Bayesian	100	105	110	115	120	125	130	135	140	145	150
Expected	1.20	1.24	1.36	1.45	1.69	1.78	1.76	1.73	1.57	1.45	1.25
Observed	0.64	0.87	1.02	1.56	1.95	2.54	2.23	2.41	2.07	1.92	1.93
CL <sub>S</sub>	100	105	110	115	120	125	130	135	140	145	150
Expected	1.17	1.24	1.36	1.50	1.66	1.73	1.78	1.69	1.56	1.39	1.20
Observed	0.61	0.86	1.06	1.64	2.05	2.72	2.38	2.53	2.07	1.90	1.79

We also show in Figure 6 and list in Table VII the observed 1-CL<sub>S</sub> and its expected distribution for the background-only hypothesis as a function of the Higgs boson mass. This is directly interpreted as the level of exclusion of our search. This figure is obtained using the CL<sub>S</sub> method.

In summary, we combine all available CDF and D0 results on SM Higgs boson searches, based on luminosities ranging from 2.1 to 6.7 fb<sup>-1</sup>. Compared to our previous combination, more data have been added to the existing channels, additional channels have been included, and analyses have been further optimized to gain sensitivity. We use the latest parton distribution functions and  $gg \rightarrow H$  theoretical cross sections when comparing our limits to the SM predictions at high mass.

The 95% C.L. upper limits on Higgs boson production are a factor of 1.56 and 0.68 times the SM cross section for a Higgs boson mass of  $m_H = 115$  and 165 GeV/ $c^2$ , respectively. Based on simulation, the corresponding median expected upper limits are 1.45 and 0.76, respectively. Standard Model branching ratios, calculated as functions of the

Higgs boson mass, are assumed.

We choose to use the intersections of piecewise linear interpolations of our observed and expected rate limits in order to quote ranges of Higgs boson masses that are excluded and that are expected to be excluded. The sensitivities of our searches to Higgs bosons are smooth functions of the Higgs boson mass and depend most strongly on the predicted cross sections and the decay branching ratios (the decay  $H \rightarrow W^+W^-$  is the dominant decay for the region of highest sensitivity). The mass resolution of the channels is poor due to the presence of two highly energetic neutrinos in signal events. We therefore use the linear interpolations to extend the results from the  $5 \text{ GeV}/c^2$  mass grid investigated to points in between. This procedure yields higher expected and observed interpolated limits than if the full dependence of the cross section and branching ratio were included as well, since the latter produces limit curves that are concave upwards. The regions of Higgs boson masses excluded at the 95% C.L. thus obtained are  $158 < m_H < 175 \text{ GeV}/c^2$  and  $100 < m_H < 109 \text{ GeV}/c^2$ . The expected exclusion region, given the current sensitivity, is  $156 < m_H < 173 \text{ GeV}/c^2$ . The excluded region obtained by finding the intersections of the linear interpolations of

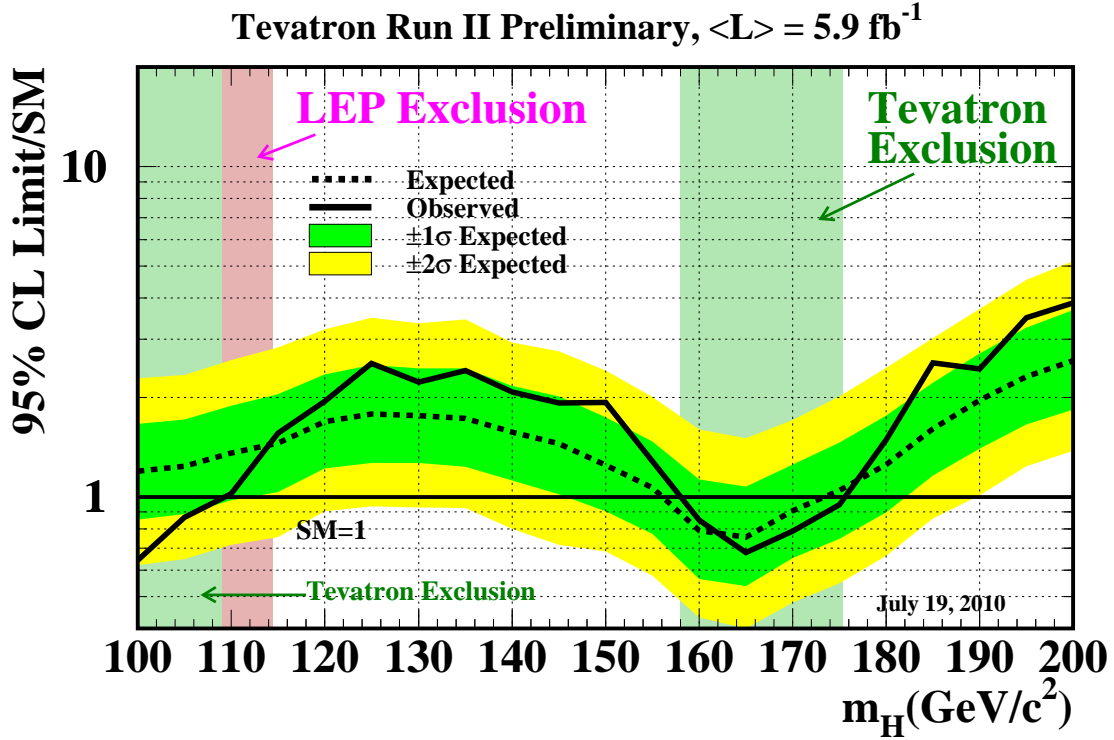


FIG. 5: Observed and expected (median, for the background-only hypothesis) 95% C.L. upper limits on the ratios to the SM cross section, as functions of the Higgs boson mass for the combined CDF and D0 analyses. The limits are expressed as a multiple of the SM prediction for test masses (every  $5 \text{ GeV}/c^2$ ) for which both experiments have performed dedicated searches in different channels. The points are joined by straight lines for better readability. The bands indicate the 68% and 95% probability regions where the limits can fluctuate, in the absence of signal. The limits displayed in this figure are obtained with the Bayesian calculation.

TABLE VI: Ratios of median expected and observed 95% C.L. limit to the SM cross section for the combined CDF and D0 analyses as a function of the Higgs boson mass in  $\text{GeV}/c^2$ , obtained with the Bayesian and with the  $\text{CL}_s$  method.

Bayesian	155	160	165	170	175	180	185	190	195	200
Expected	1.07	0.79	0.76	0.91	1.04	1.25	1.61	1.96	2.31	2.58
Observed	1.28	0.85	0.68	0.79	0.95	1.49	2.55	2.44	3.49	3.87

$\text{CL}_s$	155	160	165	170	175	180	185	190	195	200
Expected	1.05	0.77	0.73	0.89	1.04	1.25	1.59	1.96	2.32	2.66
Observed	1.26	0.84	0.69	0.77	0.93	1.43	2.46	2.29	3.44	3.80

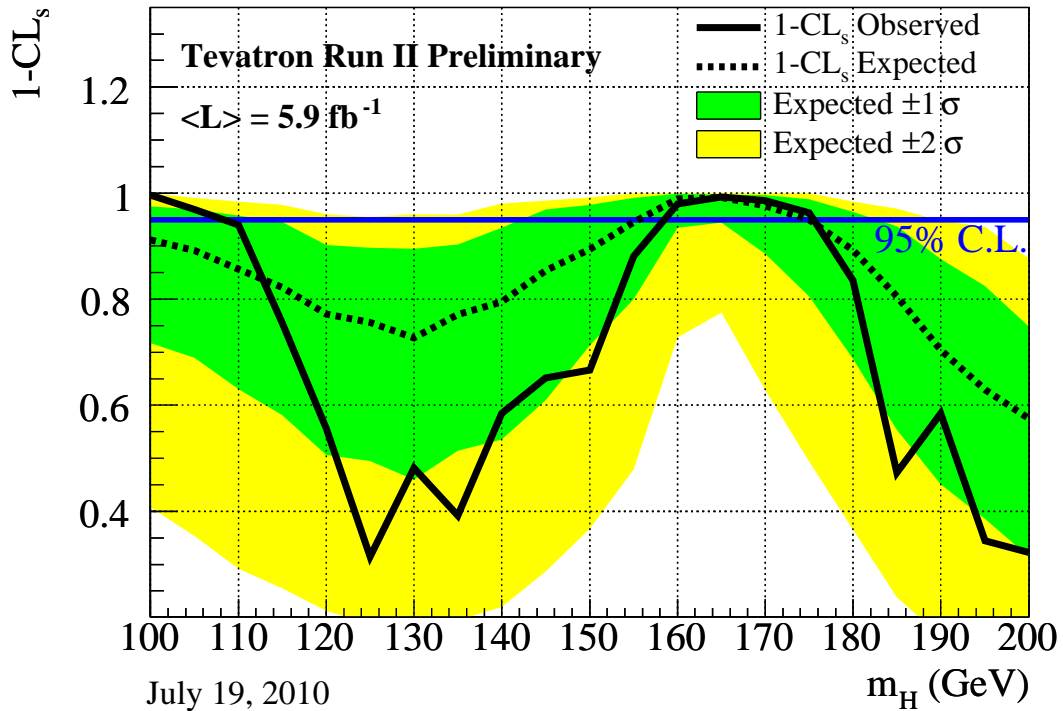


FIG. 6: The exclusion strength  $1 - \text{CL}_s$  as a function of the Higgs boson mass (in steps of  $5 \text{ GeV}/c^2$ ), as obtained with  $\text{CL}_s$  method for the combination of the CDF and D0 analyses.

the observed  $1 - \text{CL}_s$  curve shown in Figure 6 is slightly larger than that obtained with the Bayesian calculation. As previously stated, we make the *a priori* choice to quote the exclusion region using the Bayesian calculation.

The results presented in this paper significantly extend the individual limits of each collaboration and those obtained in our previous combination. The sensitivity of our combined search is sufficient to exclude a Higgs boson at high mass and is expected to grow substantially in the future as more data are added and further improvements are made to our analysis techniques.



TABLE VII: The observed and expected 1-CL<sub>s</sub> values as functions of  $m_H$ , for the combined CDF and D0 Higgs boson searches.

$m_H$ (GeV/ $c^2$ )	1-CL <sub>s</sub> <sup>obs</sup>	1-CL <sub>s</sub> <sup>-2σ</sup>	1-CL <sub>s</sub> <sup>-1σ</sup>	1-CL <sub>s</sub> <sup>median</sup>	1-CL <sub>s</sub> <sup>+1σ</sup>	1-CL <sub>s</sub> <sup>+2σ</sup>
100	0.996	1.000	0.975	0.912	0.717	0.408
105	0.969	0.991	0.969	0.892	0.689	0.353
110	0.940	0.984	0.958	0.856	0.630	0.292
115	0.754	0.978	0.945	0.822	0.581	0.254
120	0.556	0.960	0.902	0.772	0.506	0.213
125	0.315	0.955	0.896	0.756	0.495	0.187
130	0.482	0.960	0.895	0.727	0.460	0.183
135	0.392	0.959	0.903	0.771	0.514	0.195
140	0.585	0.981	0.934	0.795	0.535	0.219
145	0.652	0.986	0.968	0.853	0.609	0.286
150	0.667	0.992	0.977	0.894	0.713	0.367
155	0.881	1.000	0.991	0.945	0.800	0.479
160	0.979	1.000	0.998	0.989	0.935	0.728
165	0.993	1.000	0.997	0.991	0.944	0.774
170	0.986	1.000	0.996	0.976	0.885	0.629
175	0.963	1.000	0.988	0.950	0.805	0.494
180	0.835	0.984	0.965	0.892	0.688	0.365
185	0.473	0.971	0.937	0.805	0.554	0.238
190	0.585	0.948	0.876	0.705	0.451	0.163
195	0.345	0.936	0.825	0.630	0.386	0.130
200	0.323	0.876	0.748	0.575	0.315	0.100

- 
- [1] CDF Collaboration, “Combined Upper Limit on Standard Model Higgs Boson Production for ICHEP 2010”, CDF Conference Note 10241 (2010).
- [2] “Combined Upper Limits on Standard Model Higgs Boson Production from the D0 Experiment in up to 6.7 fb<sup>-1</sup> of data”, D0 Conference Note 6094 (2010).
- [3] CDF Collaboration, “Combined Upper Limit on Standard Model Higgs Boson Production for HCP 2009”, CDF Conference Note 9999 (2009). CDF Collaboration, “Combined Upper Limit on Standard Model Higgs Boson Production for Summer 2009”, CDF Conference Note 9807 (2009); D0 Collaboration, “Combined Upper Limits on Standard Model Higgs Boson Production from the D0 Experiment in 2.1-5.4 fb<sup>-1</sup>”, D0 Conference Note 6008 (2009). D0 Collaboration, “Combined upper limits on Standard Model Higgs boson production from the D0 experiment in 0.9-5.0 fb<sup>-1</sup>”, D0 Conference Note 5984 (2009); The CDF and D0 Collaborations and the TEVNPBWG Working Group, “Combined CDF and DZero Upper Limits on Standard Model Higgs-Boson Production with 2.1 to 4.2 fb<sup>-1</sup> of Data”, FERMILAB-PUB-09-0557-E, CDF Note 9998, D0 Note 5983, arXiv:0911.3930v1 [hep-ex] (2009).
- [4] CDF Collaboration, “Inclusive Search for Standard Model Higgs Boson Production in the WW Decay Channel Using the CDF II Detector”, Phys. Rev. Lett. 104, 061803 (2010); D0 Collaboration, “Search for Higgs Boson Production in Dilepton and Missing Energy Final States with 5.4 fb<sup>-1</sup> of  $p\bar{p}$  Collisions at  $\sqrt{s} = 1.96$  TeV”, Phys. Rev. Lett. 104, 061804 (2010); The CDF and D0 Collaborations, “Combination of Tevatron Searches for the Standard Model Higgs Boson in the  $W^+W^-$  Decay Mode”, Phys. Rev. Lett. 104, 061802 (2010).
- [5] CDF Collaboration, “Search for Standard Model Higgs boson production in association with a  $W$  boson using Neural Network techniques with 5.7 fb<sup>-1</sup>”, CDF Conference Note 10239 (2010).
- [6] CDF Collaboration, “Search for Standard Model Higgs boson production in association with a  $W$  boson using Matrix Element techniques with 5.6 fb<sup>-1</sup> of CDF Data”, CDF Conference Note 10217 (2010).
- [7] CDF Collaboration, “Search for the Standard Model Higgs boson in the  $\cancel{E}_T$  plus jets sample”, CDF Conference Note 10212 (2010).
- [8] CDF Collaboration, “A Search for the Standard Model Higgs boson in the process  $ZH \rightarrow \ell^+\ell^-b\bar{b}$  using 5.7 fb<sup>-1</sup> of CDF II Data”, CDF Conference Note 10235 (2010).
- [9] CDF Collaboration, “A Search for the Standard Model Higgs boson in the process  $ZH \rightarrow \ell^+\ell^-b\bar{b}$  using a loosened muon selection”, CDF Conference Note 10221 (2010).
- [10] CDF Collaboration, “Search for  $H \rightarrow WW^*$  Production Using 5.9 fb<sup>-1</sup>”, CDF Conference Note 10232 (2010).
- [11] CDF Collaboration, “Search for a low mass Standard Model Higgs boson in the di-tau decay channel with 2.3 fb<sup>-1</sup> of CDF data”, CDF Conference Note 10133 (2010).
- [12] CDF Collaboration, “A search for the Higgs Boson in the All Hadronic Channel with Data Sample of 4 fb<sup>-1</sup>”, CDF Conference Note 10010 (2010).
- [13] CDF Collaboration, “Search for a SM Higgs Boson with the Diphoton Final State at CDF”, CDF Conference Note 10065 (2010).
- [14] D0 Collaboration, “Search for WH associated production with 5.3 fb<sup>-1</sup> of Tevatron data,” D0 Conference Note 6092.
- [15] D0 Collaboration, “Search for the standard model Higgs boson in  $\tau$  final states”, Phys. Rev. Lett. 102, 251801 (2009).
- [16] D0 Collaboration, “Search for the standard model Higgs boson in the  $\tau^+\tau^-q\bar{q}$  final state”, D0 Conference note 5845.
- [17] D0 Collaboration, “Search for the standard model Higgs boson in the  $ZH \rightarrow \nu\nu b\bar{b}$  channel in 5.2 fb<sup>-1</sup> of  $p\bar{p}$  collisions at  $\sqrt{s} = 1.96$  TeV”, Phys. Rev. Lett. 104, 071801 (2010).
- [18] D0 Collaboration, “Search for the standard model Higgs boson in the  $HZ \rightarrow b\bar{b}\nu\nu$  channel in 6.4 fb<sup>-1</sup> of  $p\bar{p}$  collisions at  $\sqrt{s} = 1.96$  TeV”, D0 Conference note 6087.
- [19] D0 Collaboration, “A Search for  $ZH \rightarrow \ell^+\ell^-b\bar{b}$  Production in 6.2 fb<sup>-1</sup> of data with the D0 detector in  $p\bar{p}$  Collisions at  $\sqrt{s} = 1.96$  TeV”, D0 Conference Note 6089.
- [20] D0 Collaboration, “Search for associated Higgs boson production with like sign leptons in  $p\bar{p}$  collisions at  $\sqrt{s} = 1.96$  TeV”, D0 Conference Note 6091.
- [21] D0 Collaboration, “Search for Higgs boson production in dilepton and missing energy final states with 5.4 fb<sup>-1</sup> of  $p\bar{p}$  collisions at  $\sqrt{s} = 1.96$  TeV”, Phys. Rev. Lett. 104, 061804 (2010).
- [22] D0 Collaboration, “Search for Higgs production in electron and muon plus missing transverse energy final states with 6.7 fb<sup>-1</sup> of  $p\bar{p}$  collisions at  $\sqrt{s} = 1.96$  TeV”, D0 Conference Note 6082.
- [23] D0 Collaboration, “A search for the standard model Higgs boson  $H \rightarrow WW \rightarrow leptons + jets$  in 5.4 fb<sup>-1</sup> of  $p\bar{p}$  collisions at  $\sqrt{s} = 1.96$  TeV”, D0 Conference Note 6095.
- [24] D0 Collaboration, “Search for the Standard Model Higgs boson in  $\gamma\gamma$  final states at D0 with 4.2 fb<sup>-1</sup> of data”, D0

Conference Note 5858.

- [25] D0 Collaboration, “Search for the standard model Higgs boson in the  $t\bar{t}H \rightarrow t\bar{t}b\bar{b}$  channel”, D0 Conference note 5739.
- [26] V. M. Abazov *et al.* [The D0 Collaboration], Nucl. Instrum. Meth. A **620**, 490 (2010).
- [27] C. Anastasiou, G. Dissertori, M. Grazzini, F. Stöckli and B. R. Webber, JHEP **0908**, 099 (2009).
- [28] C. Anastasiou, R. Boughezal and F. Petriello, JHEP **0904**, 003 (2009).
- [29] D. de Florian and M. Grazzini, Phys. Lett. B **674**, 291 (2009).
- [30] R. V. Harlander and W. B. Kilgore, Phys. Rev. Lett. **88**, 201801 (2002).
- [31] C. Anastasiou and K. Melnikov, Nucl. Phys. B **646**, 220 (2002).
- [32] V. Ravindran, J. Smith, and W. L. van Neerven, Nucl. Phys. B **665**, 325 (2003).
- [33] S. Actis, G. Passarino, C. Sturm, and S. Uccirati, Phys. Lett. B **670**, 12 (2008).
- [34] U. Aglietti, R. Bonciani, G. Degrassi, A. Vicini, “Two-loop electroweak corrections to Higgs production in proton-proton collisions”, arXiv:hep-ph/0610033v1 (2006).
- [35] S. Catani, D. de Florian, M. Grazzini and P. Nason, “Soft-gluon resummation for Higgs boson production at hadron colliders,” JHEP **0307**, 028 (2003) [arXiv:hep-ph/0306211].
- [36] A. D. Martin, W. J. Stirling, R. S. Thorne and G. Watt, Eur. Phys. J. C **63**, 189 (2009).
- [37] K. A. Assamagan *et al.* [Higgs Working Group Collaboration], “The Higgs working group: Summary report 2003,” arXiv:hep-ph/0406152.
- [38] O. Brein, A. Djouadi, and R. Harlander, Phys. Lett. B **579**, 149 (2004).
- [39] M. L. Ciccolini, S. Dittmaier, and M. Kramer, Phys. Rev. D **68**, 073003 (2003).
- [40] E. Berger and J. Campbell, Phys. Rev. D **70** 073011 (2004).
- [41] W. Beenaker, S. Dittmaier, M. Krämer, B. Plümper, M. Spira, and P. M. Zerwas, Phys. Rev. Lett. **87**, 201805 (2001); L. Reina and S. Dawson, Phys. Rev. Lett. **87**, 201804 (2001).
- [42] J. Baglio and A. Djouadi, arXiv:1003.4266 [hep-ph] (2010). We have obtained extended versions of the table of  $WH$  and  $ZH$  cross sections for all Higgs boson masses we test, and with more digits of precision, from the authors.
- [43] T. Sjöstrand, L. Lonnblad and S. Mrenna, “PYTHIA 6.2: Physics and manual,” arXiv:hep-ph/0108264.
- [44] H. L. Lai *et al.*, Phys. Rev D **55**, 1280 (1997).
- [45] A. Djouadi, J. Kalinowski and M. Spira, Comput. Phys. Commun. **108**, 56 (1998).
- [46] M. L. Mangano, M. Moretti, F. Piccinini, R. Pittau and A. D. Polosa, “ALPGEN, a generator for hard multiparton processes in hadronic collisions,” JHEP **0307**, 001 (2003).
- [47] S. Frixione and B.R. Webber, JHEP **0206**, 029 (2002).
- [48] G. Corcella *et al.*, JHEP **0101**, 010 (2001).
- [49] A. Pukhov *et al.*, “CompHEP: A package for evaluation of Feynman diagrams and integration over multi-particle phase space. User’s manual for version 33,” [arXiv:hep-ph/9908288].
- [50] J. Campbell and R. K. Ellis, <http://mcfm.fnal.gov/>.
- [51] T. Junk, Nucl. Instrum. Meth. A **434**, 435 (1999);  
A.L. Read, “Modified Frequentist analysis of search results (the CL<sub>s</sub> method)”, in F. James, L. Lyons and Y. Perrin (eds.), *Workshop on Confidence Limits*, CERN, Yellow Report 2000-005, available through [cdsweb.cern.ch](http://cdsweb.cern.ch).
- [52] W. Fisher, “Systematics and Limit Calculations,” FERMILAB-TM-2386-E.
- [53] S. Moch and P. Uwer, U. Langenfeld, S. Moch and P. Uwer, Phys. Rev. D **80**, 054009 (2009).
- [54] The CDF and D0 Collaborations and the Tevatron Electroweak Working Group, arXiv:0903.2503 [hep-ex].
- [55] M. Cacciari, S. Frixione, M. L. Mangano, P. Nason and G. Ridolfi, JHEP **0809**, 127 (2008).  
N. Kidonakis and R. Vogt, Phys. Rev. D **78**, 074005 (2008).
- [56] N. Kidonakis, Phys. Rev. D **74**, 114012 (2006).
- [57] N. Kidonakis, private communication.
- [58] N. Kidonakis, arXiv:1005.3330 [hep-ph].
- [59] B. W. Harris, E. Laenen, L. Phaf, Z. Sullivan and S. Weinzierl, Phys. Rev. D **66**, 054024 (2002).
- [60] J. Campbell and R. K. Ellis, Phys. Rev. D **65**, 113007 (2002).

# Appendices

## Appendix A: Systematic Uncertainties

TABLE VIII: Systematic uncertainties on the signal and background contributions for CDF's  $WH \rightarrow \ell\nu b\bar{b}$  tight double tag (TDT), loose double tag (LDT), looser double tag (LDTX), and single tag (ST) 2 jet channels. Systematic uncertainties are listed by name; see the original references for a detailed explanation of their meaning and on how they are derived. Systematic uncertainties for  $WH$  shown in this table are obtained for  $m_H = 115 \text{ GeV}/c^2$ . Uncertainties are relative, in percent, and are symmetric unless otherwise indicated.

CDF: tight and loose double-tag (TDT and LDT)  $WH \rightarrow \ell\nu b\bar{b}$  channel relative uncertainties (%)

Contribution	W+HF	Mistags	Top	Diboson	Non-W	WH
Luminosity ( $\sigma_{\text{inel}}(p\bar{p})$ )	0	0	3.8	3.8	0	3.8
Luminosity Monitor	0	0	4.4	4.4	0	4.4
Lepton ID	0	0	2	2	0	2
Jet Energy Scale	0	0	0	0	0	2
Mistag Rate	0	35	0	0	0	0
B-Tag Efficiency	0	0	8.6	8.6	0	8.6
$t\bar{t}$ Cross Section	0	0	10	0	0	0
Diboson Rate	0	0	0	11.5	0	0
Signal Cross Section	0	0	0	0	0	5
HF Fraction in W+jets	45	0	0	0	0	0
ISR+FSR+PDF	0	0	0	0	0	5
QCD Rate	0	0	0	0	40	0

CDF: looser double-tag (LDTX)  $WH \rightarrow \ell\nu b\bar{b}$  channel relative uncertainties (%)

Contribution	W+HF	Mistags	Top	Diboson	Non-W	WH
Luminosity ( $\sigma_{\text{inel}}(p\bar{p})$ )	0	0	3.8	3.8	0	3.8
Luminosity Monitor	0	0	4.4	4.4	0	4.4
Lepton ID	0	0	2	2	0	2
Jet Energy Scale	0	0	0	0	0	2.2
Mistag Rate	0	36	0	0	0	0
B-Tag Efficiency	0	0	13.6	13.6	0	13.6
$t\bar{t}$ Cross Section	0	0	10	0	0	0
Diboson Rate	0	0	0	11.5	0	0
Signal Cross Section	0	0	0	0	0	5
HF Fraction in W+jets	45	0	0	0	0	0
ISR+FSR+PDF	0	0	0	0	0	7.7
QCD Rate	0	0	0	0	40	0

CDF: single tag (ST)  $WH \rightarrow \ell\nu b\bar{b}$  channel relative uncertainties (%)

Contribution	W+HF	Mistags	Top	Diboson	Non-W	WH
Luminosity ( $\sigma_{\text{inel}}(p\bar{p})$ )	0	0	3.8	3.8	0	3.8
Luminosity Monitor	0	0	4.4	4.4	0	4.4
Lepton ID	0	0	2	2	0	2
Jet Energy Scale	0	0	0	0	0	2
Mistag Rate	0	35	0	0	0	0
B-Tag Efficiency	0	0	4.3	4.3	0	4.3
$t\bar{t}$ Cross Section	0	0	10	0	0	0
Diboson Rate	0	0	0	11.5	0	0
Signal Cross Section	0	0	0	0	0	5
HF Fraction in W+jets	42	0	0	0	0	0
ISR+FSR+PDF	0	0	0	0	0	3.0
QCD Rate	0	0	0	0	40	0

TABLE IX: Systematic uncertainties on the signal and background contributions for CDF's  $WH \rightarrow \ell\nu b\bar{b}$  tight double tag (TDT), loose double tag (LDT), and single tag (ST) 3 jet channels. Systematic uncertainties are listed by name; see the original references for a detailed explanation of their meaning and on how they are derived. Systematic uncertainties for  $WH$  shown in this table are obtained for  $m_H = 115 \text{ GeV}/c^2$ . Uncertainties are relative, in percent, and are symmetric unless otherwise indicated.

CDF: tight and loose double-tag (TDT and LDT)  $WH \rightarrow \ell\nu b\bar{b}$  channel relative uncertainties (%)

Contribution	$W+HF$	Mistags	Top	Diboson	Non- $W$	$WH$
Luminosity ( $\sigma_{\text{inel}}(p\bar{p})$ )	0	0	3.8	3.8	0	3.8
Luminosity Monitor	0	0	4.4	4.4	0	4.4
Lepton ID	0	0	2	2	0	2
Jet Energy Scale	0	0	0	0	0	13.5
Mistag Rate	0	9	0	0	0	0
$B$ -Tag Efficiency	0	0	8.4	8.4	0	8.4
$t\bar{t}$ Cross Section	0	0	10	0	0	0
Diboson Rate	0	0	0	10	0	0
Signal Cross Section	0	0	0	0	0	10
HF Fraction in $W$ +jets	30	0	0	0	0	0
ISR+FSR+PDF	0	0	0	0	0	21.4
QCD Rate	0	0	0	0	40	0

CDF: single tag (ST)  $WH \rightarrow \ell\nu b\bar{b}$  channel relative uncertainties (%)

Contribution	$W+HF$	Mistags	Top	Diboson	Non- $W$	$WH$
Luminosity ( $\sigma_{\text{inel}}(p\bar{p})$ )	0	0	3.8	3.8	0	3.8
Luminosity Monitor	0	0	4.4	4.4	0	4.4
Lepton ID	0	0	2	2	0	2
Jet Energy Scale	0	0	0	0	0	15.8
Mistag Rate	0	13.3	0	0	0	0
$B$ -Tag Efficiency	0	0	3.5	3.5	0	3.5
$t\bar{t}$ Cross Section	0	0	10	0	0	0
Diboson Rate	0	0	0	10	0	0
Signal Cross Section	0	0	0	0	0	10
HF Fraction in $W$ +jets	30	0	0	0	0	0
ISR+FSR+PDF	0	0	0	0	0	13.1
QCD Rate	0	0	0	0	40	0

TABLE X: Systematic uncertainties on the signal and background contributions for D0's  $WH \rightarrow \ell\nu b\bar{b}$  single (ST) and double tag (DT) channels. Systematic uncertainties are listed by name, see the original references for a detailed explanation of their meaning and on how they are derived. Systematic uncertainties for  $WH$  shown in this table are obtained for  $m_H = 115 \text{ GeV}/c^2$ . Uncertainties are relative, in percent, and are symmetric unless otherwise indicated.

D0: single tag (ST)  $WH \rightarrow \ell\nu b\bar{b}$  channel relative uncertainties (%)

Contribution	WZ/WW	Wbb/Wcc	Wjj/Wcj	$t\bar{t}$	single top	Multijet	WH
Luminosity	6	6	6	6	6	0	6
Trigger eff.	2-3	2-3	2-3	2-3	2-3	0	2-3
EM ID/Reco eff./resol.	3	3	3	3	3	0	3
Muon ID/Reco eff./resol.	4.1	4.1	4.1	4.1	4.1	0	4.1
Jet ID/Reco eff.	1	1	2	1	1	0	1
Jet Energy Scale	2-5	2-5	2-5	2-4	2-5	0	2-5
$b$ -tagging/taggability	5-6	3-4	8-9	2-4	2-4	0	2-4
Cross Section	6	9	9	10	10	0	6
Heavy-Flavor K-factor	0	20	0	0	0	0	0
Instrumental-WH	0	0	0	0	0	1	0
PDF, reweighting	0-1	0-2	2-3	2-3	0-4	0	0-1

D0: double tag (DT)  $WH \rightarrow \ell\nu b\bar{b}$  channel relative uncertainties (%)

Contribution	WZ/WW	Wbb/Wcc	Wjj/Wcj	$t\bar{t}$	single top	Multijet	WH
Luminosity	6	6	6	6	6	0	6
Trigger eff.	2-3	2-3	2-3	2-3	2-3	0	2-3
EM ID/Reco eff./resol.	3	3	3	3	3	0	3
Muon ID/Reco eff./resol.	4.1	4.1	4.1	4.1	4.1	0	4.1
Jet ID/Reco eff.	1	1	2	2	1	0	1-2
Jet Energy Scale	2-5	2-5	2-5	2-3	1-2	0	2-5
$b$ -tagging/taggability	9-11	9-11	7	11-14	11-14	0	11-14
Cross Section	6	9	9	10	10	0	6
Heavy-Flavor K-factor	0	20	0	0	0	0	0
Instrumental-WH	0	0	0	0	0	1	0
PDF, reweighting	0-1	0-1	1-2	2-3	0-1	0	0-1

TABLE XI: Systematic uncertainties on the signal and background contributions for CDF's  $WH, ZH \rightarrow \cancel{E}_T b\bar{b}$  tight double tag (TDT), loose double tag (LDT), and single tag (ST) channels. Systematic uncertainties are listed by name; see the original references for a detailed explanation of their meaning and on how they are derived. Systematic uncertainties for  $ZH$  and  $WH$  shown in this table are obtained for  $m_H = 120 \text{ GeV}/c^2$ . Uncertainties are relative, in percent, and are symmetric unless otherwise indicated.

CDF: tight double-tag (TDT)  $WH, ZH \rightarrow \cancel{E}_T b\bar{b}$  channel relative uncertainties (%)

Contribution	ZH	WH	Multijet	Top Pair	S. Top	Di-boson	W + h.f.	Z + h.f.
Luminosity	3.8	3.8		3.8	3.8	3.8	3.8	3.8
Lumi Monitor	4.4	4.4		4.4	4.4	4.4	4.4	4.4
Tagging SF	10.4	10.4		10.4	10.4	10.4	10.4	10.4
Trigger Eff. (shape)	1.0	1.2	1.1	0.7	1.1	1.6	1.7	1.3
Lepton Veto	2.0	2.0		2.0	2.0	2.0	2.0	2.0
PDF Acceptance	2.0	2.0		2.0	2.0	2.0	2.0	2.0
JES (shape)	+3.0 -3.0	+3.5 -4.7	-4.0 +3.8	+1.1 -1.1	+2.4 -4.7	+8.2 -6.1	+7.3 -11.8	+6.5 -8.3
ISR		+4.4						
FSR		+3.7 +1.8 +4.4						
Cross-Section	5	5		10	10	6	30	30
Multijet Norm. (shape)			22					

CDF: loose double-tag (LDT)  $WH, ZH \rightarrow \cancel{E}_T b\bar{b}$  channel relative uncertainties (%)

Contribution	ZH	WH	Multijet	Top Pair	S. Top	Di-boson	W + h.f.	Z + h.f.
Luminosity	3.8	3.8		3.8	3.8	3.8	3.8	3.8
Lumi Monitor	4.4	4.4		4.4	4.4	4.4	4.4	4.4
Tagging SF	11.6	11.6		11.6	11.6	11.6	11.6	11.6
Trigger Eff. (shape)	1.2	1.3	1.1	0.7	1.2	1.2	1.8	1.3
Lepton Veto	2.0	2.0		2.0	2.0	2.0	2.0	2.0
PDF Acceptance	2.0	2.0		2.0	2.0	2.0	2.0	2.0
JES (shape)	+3.7 -3.7	+4.0 -4.0	-5.4 +5.2	+1.1 -0.7	+4.2 -4.2	+7.0 -7.0	+1.3 -7.6	+6.2 -7.1
ISR		+1.4 -2.9 +5.3 +2.5						
FSR								
Cross-Section	5.0	5.0		10	10	6	30	30
Multijet Norm. (shape)			11					

CDF: single-tag (ST)  $WH, ZH \rightarrow \cancel{E}_T b\bar{b}$  channel relative uncertainties (%)

Contribution	ZH	WH	Multijet	Top Pair	S. Top	Di-boson	W + h.f.	Z + h.f.
Luminosity	3.8	3.8		3.8	3.8	3.8	3.8	3.8
Lumi Monitor	4.4	4.4		4.4	4.4	4.4	4.4	4.4
Tagging SF	5.2	5.2		5.2	5.2	5.2	5.2	5.2
Trigger Eff. (shape)	0.9	1.1	1.1	0.7	1.1	1.3	2.0	1.4
Lepton Veto	2.0	2.0		2.0	2.0	2.0	2.0	2.0
PDF Acceptance	2.0	2.0		2.0	2.0	2.0	2.0	2.0
JES (shape)	+3.8 -3.8	+3.8 -3.8	-5.2 +5.6	+0.7 -0.8	+4.6 -4.6	+7.0 -5.6	+12.4 -12.7	+8.3 -8.1
ISR		-1.0 -1.5 +2.0 -0.1						
FSR								
Cross-Section	5.0	5.0		10	10	6	30	30
Multijet Norm. (shape)			10					

TABLE XII: Systematic uncertainties on the signal and background contributions for D0's  $ZH \rightarrow \nu\nu b\bar{b}$  single tag (ST) and tight-loose double tag (TLDT) channels. Systematic uncertainties are listed by name; see the original references for a detailed explanation of their meaning and on how they are derived. Systematic uncertainties for  $ZH$ ,  $WH$  shown in this table are obtained for  $m_H = 115 \text{ GeV}/c^2$ . Uncertainties are relative, in percent, and are symmetric unless otherwise indicated. Shape uncertainties are labeled with an "s".

D0: single tag (ST)  $ZH \rightarrow \nu\nu b\bar{b}$  channel relative uncertainties (%)

Contribution	WZ/ZZ	Z+jets	W+jets	$t\bar{t}$	ZH,WH
Jet Energy Scale pos/neg (S)	$\pm 5.5$	$\pm 5.5$	$\pm 7.0$	$\mp 1.5$	$\pm 1.9$
Jet ID (S)	1.1	0.7	1.0	0.8	0.7
Jet Resolution pos/neg (S)	$\pm 0.5$	$\pm 2.7$	$\pm 3.8$	$\mp 0.6$	$\pm 0.7$
MC Heavy flavor $b$ -tagging pos/neg (S)	$\pm 4.5$	$\pm 2.9$	$\pm 2.8$	$\pm 3.5$	$\pm 3.5$
MC light flavor $b$ -tagging pos/neg (S)	$\pm 3.1$	$\pm 4.9$	$\pm 6.5$	$\pm 0.6$	$\pm 0.1$
Direct taggability (S)	1.6	1.3	1.7	0.5	1.9
Trigger efficiency (S)	3.5	3.5	3.5	3.5	3.5
ALPGEN MLM pos/neg(S)	-	Shape Only	Shape only	-	-
ALPGEN Scale (S)	-	Shape Only	Shape only	-	-
Underlying Event (S)	-	Shape Only	Shape only	-	-
Parton Distribution Function (S)	0.0	0.4	0.2	2.0	0.0
EM ID	0.3	0	0.3	0.6	1.0
Muon ID	1.1	0.5	1.4	1.9	0.2
Cross Section	7	6.0	6.0	10	6.0
Heavy Flavor Ratio	-	20	20	-	-
Luminosity	6.1	6.1	6.1	6.1	6.1

D0: double tag (TLDT)  $ZH \rightarrow \nu\nu b\bar{b}$  channel relative uncertainties (%)

Contribution	WZ/ZZ	Z+jets	W+jets	$t\bar{t}$	ZH,WH
Jet Energy Scale pos/neg (S)	$\pm 5.1$	$\pm 7.1$	$\pm 6.6$	$\mp 0.5$	$\pm 1.6$
Jet ID (S)	1.1	$\pm 1.2$	0.8	0.1	1.1
Jet Resolution pos/neg (S)	$\mp 1.6$	$\pm 2.0$	$\pm 1.9$	$\mp 2.0$	$\mp 1.6$
MC Heavy flavor $b$ -tagging pos/neg (S)	$\pm 8.0$	$\pm 0.6$	$\pm 8.5$	$\pm 10.2$	$\pm 9.9$
MC light flavor $b$ -tagging pos/neg (S)	1.5	$\pm 12.6$	$\pm 1.2$	$\pm 0.1$	0.0
Direct taggability & Vertex Confirmation(S) pos/neg	7.4/1.5	$\pm 9.0$	$\pm 6.8$	5.2/0.1	8.3/0.0
Trigger efficiency (S)	3.5	3.5	3.5	3.5	3.5
ALPGEN MLM pos/neg (S)	-	Shape only	Shape only	-	-
ALPGEN Scale (S)	-	Shape only	Shape only	-	-
Underlying Event (S)	-	Shape only	Shape only	-	-
Parton Distribution Function (S)	$\pm 0.1$	0.0	$\pm 0.4$	0.6/-0.5	0.6/0.9
EM ID	0.3	-	0.6	0.8	0.3
Muon ID	1.1	0.5	1.0	1.8	1.0
Cross Section	7.0	6.0	6.0	10	6.0
Heavy Flavor Ratio	-	20	20	-	-
Luminosity	6.1	6.1	6.1	6.1	6.1





CDF: tight double tag (TDT) low  $s/b$   $ZH \rightarrow \ell\ell b\bar{b}$  channel relative uncertainties (%)

Contribution	Fakes	Top	$WZ$	$ZZ$	$Z + b\bar{b}$	$Z + c\bar{c}$	$Z+\text{mistag}$	$ZH$
Luminosity ( $\sigma_{\text{inel}}(p\bar{p})$ )	0	3.8	3.8	3.8	3.8	3.8	0	3.8
Luminosity Monitor	0	4.4	4.4	4.4	4.4	4.4	0	4.4
Lepton ID	0	1	1	1	1	1	0	1
Lepton Energy Scale	0	1.5	1.5	1.5	1.5	1.5	0	1.5
$ZH$ Cross Section	0	0	0	0	0	0	0	5
Fake Leptons	50	0	0	0	0	0	0	0
Jet Energy Scale (shape dep.)	0	$^{+0.5}_{-0.9}$	$^{+0.0}_{-0.0}$	$^{+0.0}_{-3.3}$	$^{+5.7}_{-6.2}$	$^{+7.2}_{-5.6}$	0	$^{+1.5}_{-0.6}$
Mistag Rate (shape dep.)	0	0	0	0	0	0	$^{+31.5}_{-27.2}$	0
B-Tag Efficiency	0	8	8	8	8	8	0	8
$t\bar{t}$ Cross Section	0	10	0	0	0	0	0	0
Diboson Cross Section	0	0	6	6	0	0	0	0
$\sigma(p\bar{p} \rightarrow Z + HF)$	0	0	0	0	40	40	0	0
ISR (shape dep.)	0	0	0	0	0	0	0	$^{-1.0}_{-2.7}$
FSR (shape dep.)	0	0	0	0	0	0	0	$^{-5.3}_{-2.8}$

CDF: loose double tag (LDT) high S/B  $ZH \rightarrow \ell\ell b\bar{b}$  channel relative uncertainties (%)

Contribution	Fakes	Top	$WZ$	$ZZ$	$Z + b\bar{b}$	$Z + c\bar{c}$	$Z+\text{mistag}$	$ZH$
Luminosity ( $\sigma_{\text{inel}}(p\bar{p})$ )	0	3.8	3.8	3.8	3.8	3.8	0	3.8
Luminosity Monitor	0	4.4	4.4	4.4	4.4	4.4	0	4.4
Lepton ID	0			1	1	1	0	1
Lepton Energy Scale	0	1.5	1.5	1.5	1.5	1.5	0	1.5
$ZH$ Cross Section	0	0	0	0	0	0	0	5
Fake Leptons	50	0	0	0	0	0	0	0
Jet Energy Scale (shape dep.)	0	$^{+1.3}_{-0.6}$	$^{+3.2}_{-4.3}$	$^{+3.2}_{-3.0}$	$^{+7.4}_{-7.3}$	$^{+6.3}_{-6.0}$	0	$^{+1.04}_{-0.6}$
Mistag Rate (shape dep.)	0	0	0	0	0	0	$^{+32.1}_{-25.7}$	0
B-Tag Efficiency	0	11	11	11	11	11	0	11
$t\bar{t}$ Cross Section	0	10	0	0	0	0	0	0
Diboson Cross Section	0	0	6	6	0	0	0	0
$\sigma(p\bar{p} \rightarrow Z + HF)$	0	0	0	0	40	40	0	0
ISR (shape dep.)	0	0	0	0	0	0	0	$^{+1.4}_{-0.6}$
FSR (shape dep.)	0	0	0	0	0	0	0	$^{+0.4}_{-2.0}$

CDF: loose double tag (LDT) low S/B  $ZH \rightarrow \ell\ell b\bar{b}$  channel relative uncertainties (%)

Contribution	Fakes	Top	$WZ$	$ZZ$	$Z + b\bar{b}$	$Z + c\bar{c}$	$Z+\text{mistag}$	$ZH$
Luminosity ( $\sigma_{\text{inel}}(p\bar{p})$ )	0	3.8	3.8	3.8	3.8	3.8	0	3.8
Luminosity Monitor	0	4.4	4.4	4.4	4.4	4.4	0	4.4
Lepton ID	0			1	1	1	0	1
Lepton Energy Scale	0	1.5	1.5	1.5	1.5	1.5	0	1.5
$ZH$ Cross Section	0	0	0	0	0	0	0	5
Fake Leptons	50	0	0	0	0	0	0	0
Jet Energy Scale (shape dep.)	0	$^{+1.7}_{-0.2}$	$^{-0.0}_{-3.4}$	$^{+3.1}_{-1.0}$	$^{+8.2}_{-8.6}$	$^{+8.0}_{-8.8}$	0	$^{+0.3}_{-1.8}$
Mistag Rate (shape dep.)	0	0	0	0	0	0	$^{+31.7}_{-26.0}$	0
B-Tag Efficiency	0	11	11	11	11	11	0	11
$t\bar{t}$ Cross Section	0	10	0	0	0	0	0	0
Diboson Cross Section	0	0	6	6	0	0	0	0
$\sigma(p\bar{p} \rightarrow Z + HF)$	0	0	0	0	40	40	0	0
ISR (shape dep.)	0	0	0	0	0	0	0	$^{+1.8}_{+5.3}$
FSR (shape dep.)	0	0	0	0	0	0	0	$^{+23.0}_{+7.9}$

TABLE XIV: Systematic uncertainties on the signal and background contributions for CDF's  $ZH \rightarrow \ell^+ \ell^- b\bar{b}$  single tag (ST), loose double tag (LDT), and tight double tag (TDT) loose muon channels. The channels are further divided to separate events collected from either the muon or missing  $E_T$  trigger path. Systematic uncertainties are listed by name; see the original references for a detailed explanation of their meaning and on how they are derived. Systematic uncertainties for  $ZH$  shown in this table are obtained for  $m_H = 115 \text{ GeV}/c^2$ . Uncertainties are relative, in percent, and are symmetric unless otherwise indicated.

CDF: single tag (ST) loose muons (muon trigger)  $ZH \rightarrow \ell b\bar{b}$  channel relative uncertainties (%)

Contribution	Fakes	Top	WZ	ZZ	$Z + b\bar{b}$	$Z + c\bar{c}$	Z+mistag	ZH
Luminosity ( $\sigma_{\text{inel}}(pp)$ )	0	3.8	3.8	3.8	3.8	3.8	0	3.8
Luminosity Monitor	0	4.4	4.4	4.4	4.4	4.4	0	4.4
Lepton ID	0	1	1	1	1	1	0	1
Lepton Energy Scale	0	1.5	1.5	1.5	1.5	1.5	0	1.5
$ZH$ Cross Section	0	0	0	0	0	0	0	5
Fake Leptons	50	0	0	0	0	0	0	0
Jet Energy Scale (shape dep.)	0	$^{+0.01}_{-0.01}$	$^{+0.0}_{-1.3}$	$^{+1.3}_{-2.1}$	$^{+2.9}_{-2.8}$	$^{+3.2}_{-2.3}$	0	$^{+0.2}_{-0.3}$
Mistag Rate (shape dep.)	0	0	0	0	0	0	$^{+14.3}_{-14.4}$	0
B-Tag Efficiency	0	4	4	4	4	4	0	4
$t\bar{t}$ Cross Section	0	10	0	0	0	0	0	0
Diboson Cross Section	0	0	6	6	0	0	0	0
$\sigma(p\bar{p} \rightarrow Z + HF)$	0	0	0	0	40	40	0	0
ISR/FSR	0	0	0	0	0	0	0	5
NN Trigger Model	0	5	5	5	5	5	0	5

CDF: loose double tag (LDT) loose muons (muon trigger)  $ZH \rightarrow \ell b\bar{b}$  channel relative uncertainties (%)

Contribution	Fakes	Top	WZ	ZZ	$Z + b\bar{b}$	$Z + c\bar{c}$	Z+mistag	ZH
Luminosity ( $\sigma_{\text{inel}}(pp)$ )	0	3.8	3.8	3.8	3.8	3.8	0	3.8
Luminosity Monitor	0	4.4	4.4	4.4	4.4	4.4	0	4.4
Lepton ID	0	1	1	1	1	1	0	1
Lepton Energy Scale	0	1.5	1.5	1.5	1.5	1.5	0	1.5
$ZH$ Cross Section	0	0	0	0	0	0	0	5
Fake Leptons	50	0	0	0	0	0	0	0
Jet Energy Scale (shape dep.)	0	$^{+0.1}_{-0.9}$	$^{+0.0}_{-0.0}$	$^{+0.0}_{-0.0}$	$^{+3.7}_{-4.2}$	$^{+4.0}_{-1.6}$	0	$^{+0.1}_{-0.0}$
Mistag Rate (shape dep.)	0	0	0	0	0	0	$^{+33.6}_{-26.2}$	0
B-Tag Efficiency	0	11	11	11	11	11	0	11
$t\bar{t}$ Cross Section	0	10	0	0	0	0	0	0
Diboson Cross Section	0	0	6	6	0	0	0	0
$\sigma(p\bar{p} \rightarrow Z + HF)$	0	0	0	0	40	40	0	0
ISR/FSR	0	0	0	0	0	0	0	3
NN Trigger Model	0	5	5	5	5	5	0	5

CDF: tight double tag (TDT) loose muons (muon trigger)  $ZH \rightarrow \ell b\bar{b}$  channel relative uncertainties (%)

Contribution	Fakes	Top	WZ	ZZ	$Z + b\bar{b}$	$Z + c\bar{c}$	Z+mistag	ZH
Luminosity ( $\sigma_{\text{inel}}(pp)$ )	0	3.8	3.8	3.8	3.8	3.8	0	3.8
Luminosity Monitor	0	4.4	4.4	4.4	4.4	4.4	0	4.4
Lepton ID	0	1	1	1	1	1	0	1
Lepton Energy Scale	0	1.5	1.5	1.5	1.5	1.5	0	1.5
$ZH$ Cross Section	0	0	0	0	0	0	0	5
Fake Leptons	50	0	0	0	0	0	0	0
Jet Energy Scale (shape dep.)	0	$^{+1.2}_{-0.0}$	$^{+0.0}_{-0.0}$	$^{+0.0}_{-0.0}$	$^{+2.1}_{-3.3}$	$^{+1.3}_{-0.0}$	0	$^{+0.0}_{-0.0}$
Mistag Rate (shape dep.)	0	0	0	0	0	0	$^{+30.7}_{-26.6}$	0
B-Tag Efficiency	0	8	8	8	8	8	0	8
$t\bar{t}$ Cross Section	0	10	0	0	0	0	0	0
Diboson Cross Section	0	0	6	6	0	0	0	0
$\sigma(p\bar{p} \rightarrow Z + HF)$	0	0	0	0	40	40	0	0
ISR/FSR	0	0	0	0	0	0	0	1
NN Trigger Model	0	5	5	5	5	5	0	5

CDF: single tag (ST) loose muons (missing  $E_T$  trigger)  $ZH \rightarrow \ell b \bar{b}$  channel relative uncertainties (%)

Contribution	Fakes	Top	$WZ$	$ZZ$	$Z + b\bar{b}$	$Z + c\bar{c}$	$Z + \text{mistag}$	$ZH$
Luminosity ( $\sigma_{\text{inel}}(p\bar{p})$ )	0	3.8	3.8	3.8	3.8	3.8	0	3.8
Luminosity Monitor	0	4.4	4.4	4.4	4.4	4.4	0	4.4
Lepton ID	0	1	1	1	1	1	0	1
Lepton Energy Scale	0	1.5	1.5	1.5	1.5	1.5	0	1.5
$ZH$ Cross Section	0	0	0	0	0	0	0	5
Fake Leptons	50	0	0	0	0	0	0	0
Jet Energy Scale (shape dep.)	0	$^{+0.0}_{-0.1}$	$^{+0.0}_{-0.0}$	$^{+0.6}_{-0.4}$	$^{+0.6}_{-0.7}$	$^{+0.7}_{-1.0}$	0	$^{+0.0}_{-0.2}$
Mistag Rate (shape dep.)	0	0	0	0	0	0	$^{+14.1}_{-14.1}$	0
B-Tag Efficiency	0	4	4	4	4	4	0	4
$t\bar{t}$ Cross Section	0	10	0	0	0	0	0	0
Diboson Cross Section	0	0	6	6	0	0	0	0
$\sigma(p\bar{p} \rightarrow Z + HF)$	0	0	0	0	40	40	0	0
ISR/FSR	0	0	0	0	0	0	0	3
NN Trigger Model	0	5	5	5	5	5	0	5

CDF: loose double tag (LDT) loose muons (missing  $E_T$  trigger)  $ZH \rightarrow \ell b \bar{b}$  channel relative uncertainties (%)

Contribution	Fakes	Top	$WZ$	$ZZ$	$Z + b\bar{b}$	$Z + c\bar{c}$	$Z + \text{mistag}$	$ZH$
Luminosity ( $\sigma_{\text{inel}}(p\bar{p})$ )	0	3.8	3.8	3.8	3.8	3.8	0	3.8
Luminosity Monitor	0	4.4	4.4	4.4	4.4	4.4	0	4.4
Lepton ID	0	1	1	1	1	1	0	1
Lepton Energy Scale	0	1.5	1.5	1.5	1.5	1.5	0	1.5
$ZH$ Cross Section	0	0	0	0	0	0	0	5
Fake Leptons	50	0	0	0	0	0	0	0
Jet Energy Scale (shape dep.)	0	$^{+0.0}_{-0.4}$	$^{+0.0}_{-0.0}$	$^{+0.0}_{-0.0}$	$^{+0.7}_{-0.3}$	$^{+0.0}_{-1.3}$	0	$^{+0.2}_{-0.2}$
Mistag Rate (shape dep.)	0	0	0	0	0	0	$^{+39.0}_{-29.5}$	0
B-Tag Efficiency	0	11	11	11	11	11	0	11
$t\bar{t}$ Cross Section	0	10	0	0	0	0	0	0
Diboson Cross Section	0	0	6	6	0	0	0	0
$\sigma(p\bar{p} \rightarrow Z + HF)$	0	0	0	0	40	40	0	0
ISR/FSR	0	0	0	0	0	0	0	1
NN Trigger Model	0	5	5	5	5	5	0	5

CDF: tight double tag (TDT) loose muons (missing  $E_T$  trigger)  $ZH \rightarrow \ell b \bar{b}$  channel relative uncertainties (%)

Contribution	Fakes	Top	$WZ$	$ZZ$	$Z + b\bar{b}$	$Z + c\bar{c}$	$Z + \text{mistag}$	$ZH$
Luminosity ( $\sigma_{\text{inel}}(p\bar{p})$ )	0	3.8	3.8	3.8	3.8	3.8	0	3.8
Luminosity Monitor	0	4.4	4.4	4.4	4.4	4.4	0	4.4
Lepton ID	0	1	1	1	1	1	0	1
Lepton Energy Scale	0	1.5	1.5	1.5	1.5	1.5	0	1.5
$ZH$ Cross Section	0	0	0	0	0	0	0	5
Fake Leptons	50	0	0	0	0	0	0	0
Jet Energy Scale (shape dep.)	0	$^{+0.0}_{-0.0}$	$^{+0.0}_{-0.0}$	$^{+0.0}_{-0.0}$	$^{+0.4}_{-0.3}$	$^{+0.3}_{-0.1}$	0	$^{+0.5}_{-0.5}$
Mistag Rate (shape dep.)	0	0	0	0	0	0	$^{+29.7}_{-25.8}$	0
B-Tag Efficiency	0	8	8	8	8	8	0	8
$t\bar{t}$ Cross Section	0	10	0	0	0	0	0	0
Diboson Cross Section	0	0	6	6	0	0	0	0
$\sigma(p\bar{p} \rightarrow Z + HF)$	0	0	0	0	40	40	0	0
ISR/FSR	0	0	0	0	0	0	0	4
NN Trigger Model	0	5	5	5	5	5	0	5

TABLE XV: Systematic uncertainties on the contributions for D0's  $ZH \rightarrow \ell^+ \ell^- b\bar{b}$  channels. Systematic uncertainties are listed by name; see the original references for a detailed explanation of their meaning and on how they are derived. Systematic uncertainties for  $ZH$  shown in this table are obtained for  $m_H = 115 \text{ GeV}/c^2$ . Uncertainties are relative, in percent, and are symmetric unless otherwise indicated. Shape uncertainties are labeled with an "s".

D0: $ZH \rightarrow \ell b\bar{b}$ analyses relative uncertainties (%)							
Contribution	Signal	Multijet	Z+LF	$Zb\bar{b}$	$Zc\bar{c}$	Diboson	$t\bar{t}$
hline Jet Energy Scale (S)	3.8		2.1	3.5	3.8	4.8	3.3
Jet Energy Resolution (S)	3.5		4.4	10	9.5	3.9	3.6
Jet ID (S)	0.53		0.83	0.40	0.08	0.85	0.68
Taggability (S)	3.5		2.6	1.9	2.6	4.7	3.5
$Z_{p_T}$ Model (S)			4.4	4.5	4.5		
HF Tagging Efficiency (S)	1.6			3.7	6.4	6.9	1.3
LF Tagging Efficiency (S)		52	49			6.9	
$ee$ Multijet Shape (S)		13					
Multijet Normalization		20-50					
Z+jets Jet Angles (S)			0.87	0.52	0.49		
AlpGen MLM (S)			0.36				
AlpGen Scale (S)			0.23	0.16	0.15		
Underlying Event (S)			0.01	0.06	0.14		
Modeling (S)	3		2	2	2	2	7
Trigger (S)	0.52		0.64	0.41	0.38	0.49	0.69
Cross Sections	6.0			20	20	7	10
Normalization	11-14		2-10	2-10	2-10	10-15	10-15
PDFs	0.55		1	2.4	1.1	0.66	5.9

D0: Double Tag (DT)  $ZH \rightarrow \ell b\bar{b}$  analysis relative uncertainties (%)

Contribution	Signal	Multijet	Z+LF	$Zb\bar{b}$	$Zc\bar{c}$	Diboson	$t\bar{t}$
Jet Energy Scale (S)	3.7		4.6	5.2	5.4	4.9	3.2
Jet Energy Resolution(S)	2.6		10	13	12	3.2	2.9
JET ID (S)	1.4		3.0	1.0	1.4	2.2	0.96
Taggability (S)	6.2		4.3	4.5	4.4	6.8	6.4
$Z_{p_T}$ Model (S)			4.4	4.2	4.2		
HF Tagging Efficiency (S)	8.3			7.7	9.9	8.4	8.9
LF Tagging Efficiency (S)		36	15			8.4	
$ee$ Multijet Shape (S)		7.9					
Multijet Normalization		20-50					
Z+jets Jet Angles (S)			1.4	0.59	0.83		
AlpGen MLM (S)			0.33				
AlpGen Scale (S)			0.29	0.15	0.16		
Underlying Event(S)			0.05	0.11	0.16		
Modeling (S)	2		0.6	2	2	2	6
Trigger (S)	0.62		1.3	0.55	0.74	0.70	0.86
Cross Sections	6.0			20	20	7	10
Normalization	11-14		2-10	2-10	2-10	10-15	10-15
PDFs	0.55		1	2.4	1.1	0.66	5.9

TABLE XVI: Systematic uncertainties on the signal and background contributions for CDF's  $H \rightarrow W^+W^- \rightarrow \ell^\pm \ell'^\mp$  channels with zero, one, and two or more associated jets. These channels are sensitive to gluon fusion production (all channels) and  $WH, ZH$  and VBF production. Systematic uncertainties are listed by name (see the original references for a detailed explanation of their meaning and on how they are derived). Systematic uncertainties for  $H$  shown in this table are obtained for  $m_H = 160$  GeV/ $c^2$ . Uncertainties are relative, in percent, and are symmetric unless otherwise indicated. The uncertainties associated with the different background and signal processed are correlated within individual jet categories unless otherwise noted. Boldface and italics indicate groups of uncertainties which are correlated with each other but not the others on the line.

CDF:  $H \rightarrow W^+W^- \rightarrow \ell^\pm \ell'^\mp$  with no associated jet channel relative uncertainties (%)

Contribution	$WW$	$WZ$	$ZZ$	$t\bar{t}$	DY	$W\gamma$	$W+\text{jet}$	$gg \rightarrow H$	$WH$	$ZH$	VBF
<b>Cross Section :</b>											
Scale								7.0			
PDF Model								7.6			
Total	<i>6.0</i>	<i>6.0</i>	<i>6.0</i>	10.0					<b>5.0</b>	<b>5.0</b>	10.0
<b>Acceptance :</b>											
Scale (leptons)								1.7			
Scale (jets)	<i>0.3</i>							1.5			
PDF Model (leptons)								2.7			
PDF Model (jets)	<i>1.1</i>							5.5			
Higher-order Diagrams		<i>10.0</i>	<i>10.0</i>	10.0		10.0			<b>10.0</b>	<b>10.0</b>	<b>10.0</b>
$\cancel{E}_T$ Modeling					19.5						
Conversion Modeling						10.0					
Jet Fake Rates											
(Low S/B)								22.0			
(High S/B)								25.0			
Jet Energy Scale	<i>2.6</i>	<i>6.1</i>	<i>3.4</i>	<i>26.0</i>	<i>17.5</i>	<i>3.1</i>		<i>5.0</i>	<i>10.5</i>	<i>5.0</i>	<i>11.5</i>
Lepton ID Efficiencies	<i>3.0</i>	<i>3.0</i>	<i>3.0</i>	<i>3.0</i>	<i>3.0</i>			<i>3.0</i>	<i>3.0</i>	<i>3.0</i>	<i>3.0</i>
Trigger Efficiencies	<i>2.0</i>	<i>2.0</i>	<i>2.0</i>	<i>2.0</i>	<i>2.0</i>			<i>2.0</i>	<i>2.0</i>	<i>2.0</i>	<i>2.0</i>
<b>Luminosity</b>	<i>3.8</i>	<i>3.8</i>	<i>3.8</i>	<i>3.8</i>	<i>3.8</i>			<i>3.8</i>	<i>3.8</i>	<i>3.8</i>	<i>3.8</i>
<b>Luminosity Monitor</b>	<i>4.4</i>	<i>4.4</i>	<i>4.4</i>	<i>4.4</i>	<i>4.4</i>			<i>4.4</i>	<i>4.4</i>	<i>4.4</i>	<i>4.4</i>

CDF:  $H \rightarrow W^+W^- \rightarrow \ell^\pm \ell'^\mp$  with one associated jet channel relative uncertainties (%)

Contribution	$WW$	$WZ$	$ZZ$	$t\bar{t}$	DY	$W\gamma$	$W+\text{jet}$	$gg \rightarrow H$	$WH$	$ZH$	VBF
<b>Cross Section :</b>											
Scale								23.5			
PDF Model								17.3			
Total	<i>6.0</i>	<i>6.0</i>	<i>6.0</i>	10.0					<b>5.0</b>	<b>5.0</b>	10.0
<b>Acceptance :</b>											
Scale (leptons)								2.2			
Scale (jets)	<i>-4.0</i>							-1.9			
PDF Model (leptons)								3.6			
PDF Model (jets)	<i>4.7</i>							-6.3			
Higher-order Diagrams		<i>10.0</i>	<i>10.0</i>	10.0		10.0			<b>10.0</b>	<b>10.0</b>	<b>10.0</b>
$\cancel{E}_T$ Modeling					20.0						
Conversion Modeling						10.0					
Jet Fake Rates											
(Low S/B)								23.0			
(High S/B)								28.0			
Jet Energy Scale	<i>-5.5</i>	<i>-1.0</i>	<i>-4.3</i>	<i>-13.0</i>	<i>-6.5</i>	<i>-9.5</i>		<i>-4.0</i>	<i>-8.5</i>	<i>-7.0</i>	<i>-6.5</i>
Lepton ID Efficiencies	<i>3.0</i>	<i>3.0</i>	<i>3.0</i>	<i>3.0</i>	<i>3.0</i>			<i>3.0</i>	<i>3.0</i>	<i>3.0</i>	<i>3.0</i>
Trigger Efficiencies	<i>2.0</i>	<i>2.0</i>	<i>2.0</i>	<i>2.0</i>	<i>2.0</i>			<i>2.0</i>	<i>2.0</i>	<i>2.0</i>	<i>2.0</i>
<b>Luminosity</b>	<i>3.8</i>	<i>3.8</i>	<i>3.8</i>	<i>3.8</i>	<i>3.8</i>			<i>3.8</i>	<i>3.8</i>	<i>3.8</i>	<i>3.8</i>
<b>Luminosity Monitor</b>	<i>4.4</i>	<i>4.4</i>	<i>4.4</i>	<i>4.4</i>	<i>4.4</i>			<i>4.4</i>	<i>4.4</i>	<i>4.4</i>	<i>4.4</i>

CDF:  $H \rightarrow W^+W^- \rightarrow \ell^\pm \ell'^\mp$  with two or more associated jets channel relative uncertainties (%)

Contribution	$WW$	$WZ$	$ZZ$	$t\bar{t}$	DY	$W\gamma$	$W+\text{jet}$	$gg \rightarrow H$	$WH$	$ZH$	VBF
<b>Cross Section :</b>											
Scale								67.5			
PDF Model								29.7			
Total	<i>6.0</i>	<i>6.0</i>	<i>6.0</i>	10.0					<b>5.0</b>	<b>5.0</b>	10.0
<b>Acceptance :</b>											
Scale (leptons)								3.1			
Scale (jets)	-8.2							-6.8			
PDF Model (leptons)								4.8			
PDF Model (jets)	4.2							-12.3			
Higher-order Diagrams		10.0	10.0	10.0		10.0			<b>10.0</b>	<b>10.0</b>	<b>10.0</b>
$\cancel{E}_T$ Modeling					25.5						
Conversion Modeling						10.0					
Jet Fake Rates							28.0				
Jet Energy Scale	-14.8	-12.9	-12.1	-1.7	-29.2	-22.0		-17.0	-4.0	-2.3	-4.0
$b$ -tag Veto				3.8							
Lepton ID Efficiencies	3.0	3.0	3.0	3.0	3.0			3.0	3.0	3.0	3.0
Trigger Efficiencies	2.0	2.0	2.0	2.0	2.0			2.0	2.0	2.0	2.0
<b>Luminosity</b>	<i>3.8</i>	<i>3.8</i>	<i>3.8</i>	<i>3.8</i>	<i>3.8</i>			<i>3.8</i>	<i>3.8</i>	<i>3.8</i>	<i>3.8</i>
<b>Luminosity Monitor</b>	<i>4.4</i>	<i>4.4</i>	<i>4.4</i>	<i>4.4</i>	<i>4.4</i>			<i>4.4</i>	<i>4.4</i>	<i>4.4</i>	<i>4.4</i>

TABLE XVII: Systematic uncertainties on the signal and background contributions for CDF's low- $M_{\ell\ell}$   $H \rightarrow W^+W^- \rightarrow \ell^\pm \ell'^\mp$  channel with zero or one associated jets. This channel is sensitive to only gluon fusion production. Systematic uncertainties are listed by name (see the original references for a detailed explanation of their meaning and on how they are derived). Systematic uncertainties for  $H$  shown in this table are obtained for  $m_H = 160$  GeV/ $c^2$ . Uncertainties are relative, in percent, and are symmetric unless otherwise indicated. The uncertainties associated with the different background and signal processed are correlated within individual categories unless otherwise noted. In these special cases, the correlated uncertainties are shown in either italics or bold face text.

CDF: low  $M_{\ell\ell}$   $H \rightarrow W^+W^- \rightarrow \ell^\pm \ell'^\mp$  with zero or one associated jets channel relative uncertainties (%)

Contribution	$WW$	$WZ$	$ZZ$	$t\bar{t}$	DY	$W\gamma$	$W+\text{jet}(s)$	$gg \rightarrow H$
<b>Cross Section :</b>								
Scale								12.0
PDF Model								10.7
Total	<i>6.0</i>	<i>6.0</i>	<i>6.0</i>	10.0	5.0			16.1
<b>Acceptance :</b>								
Scale (leptons)								0.6
Scale (jets)								1.2
PDF Model (leptons)								1.0
PDF Model (jets)	1.6							2.1
Higher-order Diagrams		10.0	10.0	10.0	10.0			
Jet Energy Scale	1.0	2.3	2.0	12.9	6.4	1.3		2.4
Conversion Modeling						10.0		
Jet Fake Rates							18.4	
Lepton ID Efficiencies	3.0	3.0	3.0	3.0	3.0			3.0
Trigger Efficiencies	2.0	2.0	2.0	2.0	2.0			2.0
<b>Luminosity</b>	<i>3.8</i>	<i>3.8</i>	<i>3.8</i>	<i>3.8</i>	<i>3.8</i>			<i>3.8</i>
<b>Luminosity Monitor</b>	<i>4.4</i>	<i>4.4</i>	<i>4.4</i>	<i>4.4</i>	<i>4.4</i>			<i>4.4</i>





TABLE XIX: Systematic uncertainties on the signal and background contributions for CDF's  $WH \rightarrow WWW \rightarrow \ell^\pm \ell'^\pm$  channel with one or more associated jets and  $WH \rightarrow WWW \rightarrow \ell^\pm \ell'^\pm \ell''^\mp$  channel. These channels are sensitive to only  $WH$  and  $ZH$  production. Systematic uncertainties are listed by name (see the original references for a detailed explanation of their meaning and on how they are derived). Systematic uncertainties for  $H$  shown in this table are obtained for  $m_H = 160 \text{ GeV}/c^2$ . Uncertainties are relative, in percent, and are symmetric unless otherwise indicated. The uncertainties associated with the different background and signal processed are correlated within individual categories unless otherwise noted. In these special cases, the correlated uncertainties are shown in either italics or bold face text.

CDF:  $WH \rightarrow WWW \rightarrow \ell^\pm \ell'^\pm$  channel relative uncertainties (%)

Contribution	$WW$	$WZ$	$ZZ$	$t\bar{t}$	DY	$W\gamma$	$W+\text{jet}$	$WH$	$ZH$
<b>Cross Section</b>	<i>6.0</i>	<i>6.0</i>	<i>6.0</i>	10.0	5.0			<b>5.0</b>	<b>5.0</b>
Scale (Acceptance)	<i>-6.1</i>								
PDF Model (Acceptance)	<i>5.7</i>								
Higher-order Diagrams		<i>10.0</i>	<i>10.0</i>	10.0	10.0	10.0		<b>10.0</b>	<b>10.0</b>
Conversion Modeling						10.0			
Jet Fake Rates							39.1		
Jet Energy Scale	<i>-14.0</i>	<i>-3.9</i>	<i>-2.8</i>	<i>-0.6</i>	<i>-9.3</i>	<i>-7.6</i>		<i>-1.0</i>	<i>-0.7</i>
Charge Mismeasurement Rate	<i>19.0</i>			<i>19.0</i>	<i>19.0</i>				
Lepton ID Efficiencies	<i>3.0</i>	<i>3.0</i>	<i>3.0</i>	<i>3.0</i>	<i>3.0</i>			<i>3.0</i>	<i>3.0</i>
Trigger Efficiencies	<i>2.0</i>	<i>2.0</i>	<i>2.0</i>	<i>2.0</i>	<i>2.0</i>			<i>2.0</i>	<i>2.0</i>
<b>Luminosity</b>	<i>3.8</i>	<i>3.8</i>	<i>3.8</i>	<i>3.8</i>	<i>3.8</i>			<i>3.8</i>	<i>3.8</i>
<b>Luminosity Monitor</b>	<i>4.4</i>	<i>4.4</i>	<i>4.4</i>	<i>4.4</i>	<i>4.4</i>			<i>4.4</i>	<i>4.4</i>

CDF:  $WH \rightarrow WWW \rightarrow \ell^\pm \ell'^\pm \ell''^\mp$  channel relative uncertainties (%)

Contribution	$WZ$	$ZZ$	$Z\gamma$	$t\bar{t}$	Fakes	$WH$	$ZH$
<b>Cross Section</b>	<i>6.0</i>	<i>6.0</i>	10.0	10.0		<b>5.0</b>	<b>5.0</b>
Higher-order Diagrams	<i>10.0</i>	<i>10.0</i>	15.0	10.0		<b>10.0</b>	<b>10.0</b>
Jet Energy Scale			<i>-2.7</i>				
Jet Fake Rates					24.8		
$b$ -Jet Fake Rates				27.3			
MC Run Dependence			5.0				
Lepton ID Efficiencies	<i>3.0</i>	<i>3.0</i>		<i>3.0</i>		<i>3.0</i>	<i>3.0</i>
Trigger Efficiencies	<i>2.0</i>	<i>2.0</i>		<i>2.0</i>		<i>2.0</i>	<i>2.0</i>
<b>Luminosity</b>	<i>3.8</i>	<i>3.8</i>		<i>3.8</i>		<i>3.8</i>	<i>3.8</i>
<b>Luminosity Monitor</b>	<i>4.4</i>	<i>4.4</i>		<i>4.4</i>		<i>4.4</i>	<i>4.4</i>

TABLE XX: Systematic uncertainties on the signal and background contributions for CDF's  $ZH \rightarrow ZWW \rightarrow \ell^\pm \ell^\mp \ell'^\pm$  channels with 1 jet and 2 or more jets. These channels are sensitive to only  $WH$  and  $ZH$  production. Systematic uncertainties are listed by name (see the original references for a detailed explanation of their meaning and on how they are derived). Systematic uncertainties for  $H$  shown in this table are obtained for  $m_H = 160 \text{ GeV}/c^2$ . Uncertainties are relative, in percent, and are symmetric unless otherwise indicated. The uncertainties associated with the different background and signal processed are correlated within individual categories unless otherwise noted. In these special cases, the correlated uncertainties are shown in either italics or bold face text.

CDF:  $ZH \rightarrow ZWW \rightarrow \ell^\pm \ell^\mp \ell'^\pm$  with one associated jet channel relative uncertainties (%)

Contribution	$WZ$	$ZZ$	$Z\gamma$	$t\bar{t}$	Fakes	$WH$	$ZH$
<b>Cross Section</b>	<i>6.0</i>	<i>6.0</i>	10.0	10.0		<b>5.0</b>	<b>5.0</b>
Higher-order Diagrams	<i>10.0</i>	<i>10.0</i>	15.0	10.0		<b>10.0</b>	<b>10.0</b>
Jet Energy Scale	<i>-7.6</i>	<i>-2.3</i>	<i>-5.3</i>	<i>9.4</i>		<i>-9.0</i>	<i>8.1</i>
Jet Fake Rates					25.8		
$b$ -Jet Fake Rates				42.0			
MC Run Dependence			5.0				
Lepton ID Efficiencies	<i>3.0</i>	<i>3.0</i>		<i>3.0</i>		<i>3.0</i>	<i>3.0</i>
Trigger Efficiencies	<i>2.0</i>	<i>2.0</i>		<i>2.0</i>		<i>2.0</i>	<i>2.0</i>
<b>Luminosity</b>	<i>3.8</i>	<i>3.8</i>		<i>3.8</i>		<i>3.8</i>	<i>3.8</i>
<b>Luminosity Monitor</b>	<i>4.4</i>	<i>4.4</i>		<i>4.4</i>		<i>4.4</i>	<i>4.4%</i>

CDF:  $ZH \rightarrow ZWW \rightarrow \ell^\pm \ell^\mp \ell'^\pm$  with two or more associated jets channel relative uncertainties (%)

Contribution	$WZ$	$ZZ$	$Z\gamma$	$t\bar{t}$	Fakes	$WH$	$ZH$
<b>Cross Section</b>	<i>6.0</i>	<i>6.0</i>	10.0	10.0		<b>5.0</b>	<b>5.0</b>
Higher-order Diagrams	<i>10.0</i>	<i>10.0</i>	15.0	10.0		<b>10.0</b>	<b>10.0</b>
Jet Energy Scale	<i>-17.8</i>	<i>-13.1</i>	<i>-18.2</i>	<i>-3.6</i>		<i>-15.4</i>	<i>-4.9</i>
Jet Fake Rates					25.4		
$b$ -Jet Fake Rates				22.2			
MC Run Dependence			5.0				
Lepton ID Efficiencies	<i>3.0</i>	<i>3.0</i>		<i>3.0</i>		<i>3.0</i>	<i>3.0</i>
Trigger Efficiencies	<i>2.0</i>	<i>2.0</i>		<i>2.0</i>		<i>2.0</i>	<i>2.0</i>
<b>Luminosity</b>	<i>3.8</i>	<i>3.8</i>		<i>3.8</i>		<i>3.8</i>	<i>3.8</i>
<b>Luminosity Monitor</b>	<i>4.4</i>	<i>4.4</i>		<i>4.4</i>		<i>4.4</i>	<i>4.4</i>

TABLE XXI: Systematic uncertainties on the signal and background contributions for D0's  $H \rightarrow WW \rightarrow \ell^\pm \ell'^\mp$  channels. Systematic uncertainties are listed by name; see the original references for a detailed explanation of their meaning and on how they are derived. Systematic uncertainties shown in this table are obtained for the  $m_H = 165 \text{ GeV}/c^2$  Higgs selection. Uncertainties are relative, in percent, and are symmetric unless otherwise indicated.

D0:  $H \rightarrow WW \rightarrow e^\pm e^\mp$  channel relative uncertainties (%)

Contribution	Diboson	$Z/\gamma^* \rightarrow \ell\ell$	$W + jet/\gamma$	$t\bar{t}$	Multijet	$H$
Lepton ID	6	6	6	6	–	6
Charge mis-ID	1	1	1	1	–	1
Jet Energy Scale (s)	1	1	1	1	–	1
Jet identification (s)	1	1	1	1	–	1
Cross Section	7	7	7	10	2	11
Luminosity	6	6	6	6	–	6
Modeling (s)	0	1	1	0	–	1

D0:  $H \rightarrow WW \rightarrow e^\pm \mu^\mp$  channel relative uncertainties (%)

Contribution	Diboson	$Z/\gamma^* \rightarrow \ell\ell$	$W + jet/\gamma$	$t\bar{t}$	Multijet	$H$
Trigger	2	2	2	2	–	2
Lepton ID	3	3	3	3	–	3
Momentum resolution (s)	0	3	1	0	–	0
Jet Energy Scale (s)	1	5	1	1	–	1
Jet identification (s)	1	3	1	1	–	1
Cross Section	7	7	7	10	10	11
Luminosity	6	6	6	6	–	6
Modeling (s)	1	1	3	0	0	1

D0:  $H \rightarrow WW \rightarrow \mu^\pm \mu^\mp$  channel relative uncertainties (%)

Contribution	Diboson	$Z/\gamma^* \rightarrow \ell\ell$	$W + jet/\gamma$	$t\bar{t}$	Multijet	$H$
Lepton ID	4	4	4	4	–	4
Momentum resolution (s)	1	1	2	1	–	1
Charge mis-ID	1	1	1	1	–	1
Jet Energy Scale (s)	1	1	1	1	–	1
Jet identification	1	1	3	1	–	1
Cross Section	7	7	7	10	15	11
Luminosity	6	6	6	6	–	6
Modeling	0	0	1	0	0	1

TABLE XXII: Systematic uncertainties on the signal and background contributions for D0’s  $WH \rightarrow WWW \rightarrow \ell'^{\pm}\ell'^{\pm}$  channel. Systematic uncertainties are listed by name; see the original references for a detailed explanation of their meaning and on how they are derived. Shape uncertainties are labeled with the “shape” designation. Systematic uncertainties for signal shown in this table are obtained for  $m_H = 165 \text{ GeV}/c^2$ . Uncertainties are relative, in percent, and are symmetric unless otherwise indicated.

D0:  $VH \rightarrow \ell^{\pm}\ell'^{\pm} + X$  run IIa channel relative uncertainties (%)

Contribution	WZ/ZZ	W+jet	ChargeFlip	Multijet	$VH \rightarrow llX$
Cross section	7	6	0	0	0
Normalization	4	4	0	0	0
Trigger (mumu)	0	0	0	0	2
LeptonID (ee)	8.6	8.6	0	0	8.6
LeptonID (mumu)	4	4	0	0	4
LeptonID (emu)	6.3	6.3	0	0	6.3
JetID/JES	2	2	0	0	2
Jet-Lepton Fake	0	20	0	0	0
Instrumental ( $ee$ )	0	0	0	52	44
Instrumental ( $e\mu$ )	0	0	0	0	29
Instrumental ( $\mu\mu$ )	0	0	0	155	42
Instrumental Model	-	-	shape	shape	-

D0:  $VH \rightarrow \ell^{\pm}\ell'^{\pm} + X$  run IIb channel relative uncertainties (%)

Contribution	WZ/ZZ	W+jet	ChargeFlip	Multijet	$VH \rightarrow llX$
Cross section	7	6	0	0	0
Normalization	4	4	0	0	0
Trigger (mumu)	0	0	0	0	5
LeptonID (ee)	8.6	8.6	0	0	8.6
LeptonID (mumu)	4	4	0	0	4
LeptonID (emu)	6.3	6.3	0	0	6.3
JetID/JES	2	2	0	0	2
Jet-Lepton Fake	0	20	0	0	0
Instrumental ( $ee$ )	0	0	0	23	31
Instrumental ( $e\mu$ )	0	0	0	0	19
Instrumental ( $\mu\mu$ )	0	0	0	43	28
Instrumental Model	-	-	shape	shape	-

TABLE XXIII: Systematic uncertainties on the signal and background contributions for D0's  $H \rightarrow WW^* \rightarrow lvjj$  electron and muon channels. Systematic uncertainties are listed by name; see the original references for a detailed explanation of their meaning and on how they are derived. Systematic uncertainties for  $gg \rightarrow H \rightarrow WW^* \rightarrow lvjj$  shown in this table are obtained for  $m_H = 165 \text{ GeV}/c^2$ . Uncertainties are relative, in percent, and are symmetric unless otherwise indicated. Shape uncertainties are labeled with an "s".

D0:  $H \rightarrow WW^* \rightarrow lvjj$  run IIa channel relative uncertainties (%)

Contribution	W+jets	Z+jets	Top	Diboson	ggHWWlnujj
Jet Energy Scale pos/neg (S)	Shape Only	Shape Only	7.5/21.0	10.0/8.75	5.25/5.5
Wbb Jet Energy Scale	Shape Only	-	-	-	-
Top Jet Energy Scale	-	1.8	-	-	-
Jet ID (S)	Shape Only	Shape Only	5.0	3.0	1.0
Jet Resolution pos/neg (S)	Shape Only	Shape Only	1.75/0.25	2.3/1.25	1.5/0.5
SingleMuOR Trigger (S)	$\pm 0.1$	$\pm 0.1$	$\pm 0.1$	$\pm 0.1$	$\pm 0.1$
ALPGEN MLM pos/neg(S)	Shape Only	Shape Only	-	-	-
ALPGEN Scale (S)	Shape Only	Shape Only	-	-	-
Underlying Event (S)	Shape Only	Shape Only	-	-	-
Parton Distribution Function (S)	1.6/1.9	0.6/1.25	2.0/0.9	$\pm 0.05$	1.0/1.0
EM ID	$\pm 4.0$	$\pm 4.0$	$\pm 4.0$	$\pm 4.0$	$\pm 4.0$
Muon ID	$\pm 4.0$	$\pm 4.0$	$\pm 4.0$	$\pm 4.0$	$\pm 4.0$
Cross Section	6.0	6.0	10.0	7.0	10.0
Luminosity	6.1	6.1	6.1	6.1	6.1

D0:  $H \rightarrow WW^* \rightarrow lvjj$  run IIb channel relative uncertainties (%)

Contribution	W+jets	Z+jets	Top	Diboson	ggHWWlnujj
Jet Energy Scale pos/neg (S)	Shape Only	Shape Only	$\pm 6.0$	3.25/3.5	3.25/2.0
Wbb Jet Energy Scale	Shape Only	-	-	-	-
Top Jet Energy Scale	-	1.8	-	-	-
Jet ID (S)	Shape Only	Shape Only	3.25	1.25	3.5
Jet Resolution pos/neg (S)	Shape Only	Shape Only	0.5/0.3	1.0/0.5	2.0/1.75
Vertex Confirmation (S)	Shape Only	Shape Only	3.75	3.75	4.75
SingleMuOR Trigger (S)	$\pm 0.5$	$\pm 0.5$	$\pm 0.5$	$\pm 0.25$	$\pm 0.25$
ALPGEN MLM pos/neg(S)	Shape Only	Shape Only	-	-	-
ALPGEN Scale (S)	Shape Only	Shape Only	-	-	-
Underlying Event (S)	Shape Only	Shape Only	-	-	-
Parton Distribution Function (S)	3.5/2.5	8.0/1.5	2.25/3.6	$\pm 0.25$	1.75/3.75
EM ID	$\pm 4.0$	$\pm 4.0$	$\pm 4.0$	$\pm 4.0$	$\pm 4.0$
Muon ID	$\pm 4.0$	$\pm 4.0$	$\pm 4.0$	$\pm 4.0$	$\pm 4.0$
Cross Section	6.0	6.0	10.0	7.0	10.0
Luminosity	6.1	6.1	6.1	6.1	6.1

TABLE XXIV: Systematic uncertainties on the signal and background contributions for D0's  $t\bar{t}H \rightarrow t\bar{t}b\bar{b}$  channel. The systematic uncertainties for  $ZH$ ,  $WH$  shown in this table are obtained for  $m_H = 115 \text{ GeV}/c^2$ . Systematic uncertainties are listed by name; see the original references for a detailed explanation of their meaning and on how they are derived. Uncertainties are relative, in percent, and are symmetric unless otherwise indicated.

D0:  $t\bar{t}H \rightarrow t\bar{t}b\bar{b}$  channel relative uncertainties (%)

Contribution	background	$t\bar{t}H$
Luminosity	6	6
lepton ID efficiency	2-3	2-3
Event preselection	1	1
$W$ +jet modeling	15	-
Cross Section	10-50	10

TABLE XXV: Systematic uncertainties on the signal and background contributions for CDF's  $H \rightarrow \tau^+\tau^-$  channels. Systematic uncertainties are listed by name; see the original references for a detailed explanation of their meaning and on how they are derived. Systematic uncertainties for the Higgs signal shown in these tables are obtained for  $m_H = 120 \text{ GeV}/c^2$ . Uncertainties are relative, in percent, and are symmetric unless otherwise indicated.

CDF:  $H \rightarrow \tau^+\tau^-$  channel relative uncertainties (%)

Contribution	$Z/\gamma^* \rightarrow ll$	$t\bar{t}$	diboson	fakes from SS	W+jets	$WH$	$ZH$	VBF	$gg \rightarrow H$
PDF Uncertainty	1	1	1	-	-	1.2	0.9	2.2	4.9
ISR 1 JET	-	-	-	-	-	-6.1	-1.7	-2.9	13.0
ISR $\geq 2$ JETS	-	-	-	-	-	-1.5	0.1	-2.7	15.5
FSR 1 JET	-	-	-	-	-	4.3	1.0	1.7	-5.0
FSR $\geq 2$ JETS	-	-	-	-	-	-2.1	0.4	-1.1	-5.2
JES (shape) 1 JET	6.2	-7.7	7.1	-	-	-4.8	-5.3	-3.7	5.1
JES (shape) $\geq 2$ JETS	14.2	3.2	11.7	-	-	5.4	4.8	-5.2	13.2
Cross Section or Norm. 1 JET	2.2	10	6	10	18	5	5	10	23.5
Cross Section or Norm. $\geq 2$ JETS	2.2	10	6	10	30	5	5	10	67.5
MC Acceptance	2.3	-	-	-	-	-	-	-	-
tau ID scale factor:									
$N_{obs}$	2.8	2.8	2.8	-	-	2.8	2.8	2.8	2.8
$N_{SSdata}$	-3.3	-3.3	-3.3	-	-	-3.3	-3.3	-3.3	-3.3
$N_{W+jets}$	-0.3	-0.3	-0.3	-	-	-0.3	-0.3	-0.3	-0.3
Cross section (DY)	-2.1	-2.1	-2.1	-	-	-2.1	-2.1	-2.1	-2.1
MC Acceptance (DY)	-2.2	-2.2	-2.2	-	-	-2.2	-2.2	-2.2	-2.2

TABLE XXVI: Systematic uncertainties on the signal and background contributions for CDF’s  $WH + ZH \rightarrow jjbb$  and  $VBF \rightarrow jjbb$  channels. Systematic uncertainties are listed by name; see the original references for a detailed explanation of their meaning and on how they are derived. Uncertainties with provided shape systematics are labeled with “s”. Systematic uncertainties for  $H$  shown in this table are obtained for  $m_H = 115 \text{ GeV}/c^2$ . Uncertainties are relative, in percent, and are symmetric unless otherwise indicated. The cross section uncertainties are uncorrelated with each other (except for single top and  $t\bar{t}$ , which are treated as correlated). The QCD uncertainty is also uncorrelated with other channels’ QCD rate uncertainties.

CDF:  $WH + ZH \rightarrow jjbb$  and  $VBF \rightarrow jjbb$  channel relative uncertainties (%)

Contribution	$t\bar{t}$	diboson	$W/Z$ +Jets	VH	VBF
Jet Energy Correction				7 s	7 s
PDF Modeling				2	2
SecVtx+SecVtx	7.6	7.6	7.6	7.6	7.6
SecVtx+JetProb	9.7	9.7	9.7	9.7	9.7
Luminosity	6	6	6	6	6
ISR/FSR modeling				2 s	3 s
Jet Moment				s	s
Trigger	4	4	4	4	4
QCD Interpolation				s	s
QCD MJJ Tuning				s	s
QCD Jet Moment Tuning				s	s
cross section	10	6	50		

TABLE XXVII: Systematic uncertainties on the signal and background contributions for CDF’s  $H \rightarrow \gamma\gamma$  channel. Systematic uncertainties for the Higgs signal shown in this table are obtained for  $m_H = 120 \text{ GeV}/c^2$ . Systematic uncertainties are listed by name; see the original references for a detailed explanation of their meaning and on how they are derived. Uncertainties are relative, in percent, and are symmetric unless otherwise indicated.

CDF:  $H \rightarrow \gamma\gamma$  channel relative uncertainties (%)

Contribution	background	signal
Luminosity		6
$\sigma_{ggH} / \sigma_{VH} / \sigma_{VBF}$		12 / 5 / 10
PDF		1
ISR		2
FSR		2
Energy Scale		0.1
Vertex		0.2
Conversions		0.2
Photon/Electron ID		1.0
Run Dependence		1.5
Data/MC fits		0.2
Background Shape	4	

TABLE XXVIII: Systematic uncertainties on the signal and background contributions for D0's  $H \rightarrow \gamma\gamma$  channel. Systematic uncertainties for the Higgs signal shown in this table are obtained for  $m_H = 115 \text{ GeV}/c^2$ . Systematic uncertainties are listed by name; see the original references for a detailed explanation of their meaning and on how they are derived. Uncertainties are relative, in percent, and are symmetric unless otherwise indicated.

D0:  $H \rightarrow \gamma\gamma$  channel relative uncertainties (%)

Contribution	background	signal
Luminosity	6	6
Acceptance	–	2
electron ID efficiency	2	2
electron track-match inefficiency	10–20	–
Photon ID efficiency	7	7
Photon energy scale	–	2
Acceptance	–	2
$\gamma$ -jet and jet-jet fakes	26	–
Cross Section ( $Z$ )	4	6
Background subtraction	8–14	–